LA-UR-15-28116
Approved for public release; distribution is unlimited.

Title: Simultaneous Thermal Analysis of WIPP and LANL Waste Drum Samples: A Preliminary Report

Author(s): Wayne, David M.

Intended for: Report

Issued: 2015-10-19

SIMULTANEOUS THERMAL ANALYSIS OF WIPP AND LANL WASTE DRUM SAMPLES: A PRELIMINARY REPORT

David M. Wayne: MET-1, MS E 511, LANL, Los Alamos, NM 87545
d-wayne@lanl.gov, 665-7552 (o) / 667-2547 (l)

Background

On Friday, February 14, 2014, an incident in P7R7 of the WIPP underground repository released radioactive material into the environment. The direct cause of the event was a breached transuranic (TRU) waste container, subsequently identified as Drum 68660. Photographic and other evidence indicates that the breach of 68660 was caused by an exothermic event. Subsequent investigations (Britt, 2015; Clark and Funk, 2015; Wilson et al., 2015; Clark, 2015) indicate that the combination of nitrate salts, pH neutralizing chemicals, and organic-based adsorbent represented a potentially energetic mixture.

The materials inside the breached steel drum consisted of remediated, 30- to 40-year old, Pu processing wastes from LANL. The contents were processed and repackaged in 2014. Processing activities at LANL included: 1) neutralization of acidic liquid contents, 2) sorption of the neutralized liquid, and 3) mixing of acidic nitrate salts with an absorber to meet waste acceptance criteria. The contents of 68660 and its sibling, 68685, were derived from the same parent drum, S855793. Drum S855793 originally contained ten plastic bags of acidic nitrate salts, and four bags of mixed nitrate and oxalate salts generated in 1985 by Pu recovery operations. These salts were predominantly oxalic acid, hydrated nitrate salts of Mg, Ca, and Fe, anhydrous $Na(NO_3)$, and minor amounts of anhydrous and hydrous nitrate salts of Pb, Al, K, Cr, and Ni. Other major components include sorbed water, nitric acid, dissolved nitrates, an absorbent (Swheat Scoop®) and a neutralizer (KolorSafe®). The contents of 68660 are described in greater detail in Appendix E of Wilson et al. (2015).

S855793 contained approximately two gallons of free liquids: presumably a mixture of water, nitric acid, and dissolved nitrates. The liquid was drained from the parent drum and from the salt-filled bags and neutralized using KolorSafe®; a color-indicating neutralizing agent composed of triethanolamine (TEA) and an indicator dye. The resulting near-neutral liquid was then solidified using Swheat Scoop®, and placed on top of solid "job control" waste (e.g., plastic bags and bottles, and a glove-box glove) in 68660. Swheat Scoop® absorbents are 100% wheat-derived solids, composed of starch (65-70 wt. %), proteins (14 wt. %), plus lignin, lipids, cellulosic polymers, enzymes, and an indigenous microbial population.

It is likely that the starch component in the Swheat served as the predominant fuel component in 68660, though other organics such as low-density and high-density polyethylene and polyvinyl chloride were also present. Nitrate salts and nitric acid both serve as oxidizing and nitrating agents when in contact with carbonaceous materials. If nitric acid is neutralized with TEA the corresponding nitrate salt, triethanolammonium nitrate (TEAN), is produced. TEAN is more reactive than TEA as it comprises both

the fuel (organic) and oxidizer (nitrate) in the same molecule. TEAN melts at 80 °C and decomposes exothermically beginning at about 250 °C (Bracuti, 1992).

The remaining damp acidic nitrate salts from S855793 were also combined with Swheat Scoop®. This nitrate salt / Swheat mixture was distributed between 68660 and 68685 in somewhat different configurations. In 68660, the salt mixture was placed on top of the layer of neutralized and sorbed liquid. In 68685, there were no sorbed liquids, and the salt mixture was placed directly into the bottom of the drum and overlain with a lead blanket from the parent drum (Wilson et al., 2015). The physical configuration of the wastes within 68660 may have contributed to the reactivity of the contents (Wilson et al., 2015). Wastes were situated within the drum in a manner that created several interfacial regions having contrasting chemistries and thermal conductivities: (1) solid "job control" and neutralized sorbed liquid, (2) neutralized sorbed liquid and nitrate-salt mixture, (3) neutralized sorbed liquid and polyethylene liner, (4) nitrate-salt mixture and polyethylene liner, and (5) nitrate-salt mixture and drum head space. Wastes having different compositions were situated as layers within the drum, and the resulting interface between adjacent layers of neutralized-and-sorbed liquid + organics and nitrate salt + organics may have created localized reactive zones that led to the thermal runaway event.

Table 1: Identification and physical appearance for each sample analyzed using DSC-MS

Sample ID	**Drum Number**	**Description (before run – samples ground and dried at 110 °C unless otherwise noted)**	**Description (after run)**
4174-1-6	S802701	Translucent crystals, not ground – from top layer	White-clear glassy residue
4174-2-7	S813389	White-gray powder and crusty aggregates w/darker granules –from top layer, not ground	Clear, frothy, glass-like residue
69120	S855793	Sample 1: White / tan powder & aggregates w/ black & white specks – monolith 1 scraped from emptied parent drum	Reddish brown ('nutmeg') crust
69120	S855793	Sample 2: White-tan powder w/brown flecks – monolith 2 scraped from emptied parent drum	Reddish brown ('nutmeg') powder
69120	S855793	Sample 3: Brown-gray powder w/brown & white flecks – monolith 3 scraped from emptied parent drum	Reddish brown ('nutmeg') crust
69139	S864694	Gray-tan powder w/white flecks – scraped from emptied parent drum	Reddish brown ('nutmeg') powder
68492	S822952	Brown-gray powder w/white flecks – scraped from emptied parent drum	Brick-red crust
68645	S818449	Yellowish-tan powder, slightly hygroscopic, w/white flecks – scraped from emptied parent drum	Reddish brown ('nutmeg') crust
69173	S851436	Tan-gray powder – scraped from emptied parent drum	Dark brown / black powder

An interdisciplinary study conducted by multiple DOE laboratories (Wilson et al., 2015) concluded: "*The physical evidence from P7R7, combined with thorough analysis of available sample data, chemical reactivity testing, and analytical modeling, indicates that Drum 68660 breached as a result of internal reactions that were exothermic in nature. The Technical Assessment Team (TAT) hypothesizes that a sequence of exothermic chemical reactions led to a thermal runaway, which resulted in solids, radioactivity, and hot gases being released from the drum.*"

The report also concludes that the contents of 68660 did not detonate. Rather, the breach was the result of "…*internal chemical reactions that generated heat and produced gases that built up pressure sufficient to overcome the drum vent and seal*." Thermal analyses of samples from 68660 were an important part of the data set in Wilson et al. (2015), but these did not include DSC measurements. While we had no access to samples from drum 68660, samples from its parent (S855793) were available to us. We also analyzed analogous materials sampled from four different drums that had similar contents and age.

A Brief Description of the Samples

Samples analyzed for this study fall into four broad categories (Table 1).

1. Pure nitrate and nitrate hydrate salts (Na, K, Pb, Mg, Fe^{3+}), and calcium oxalate hydrate.
2. Samples of nitrate salts taken from the top layer of waste inside two full parent drums. (S802701 and S813389) that had never been processed. These are referred to as "top layer salts" in this report.
3. Salts scooped out of the bottom of four parent drums that had been emptied at WCRRF. These are referred to as "residual salts" in this report.
4. Three "monolith" samples labelled 69120 (1-3) are residual salts from drum S855793, the parent of 68660. These samples consist of discrete chunks of solid material found in the material scraped from the interior of the drum.

We performed simultaneous thermal analysis and mass spectrometry of the offgas (STA-MS) on pure reagent-grade Na, Pb, Mg, Fe (III), and K nitrates and Ca oxalate obtained from known sources from within LANL's Chemistry and Manufacturing Engineering Technologies divisions in order to compare the thermal behavior of these compounds with that of the mixtures found in the various waste forms.

Top layer salts are comprised of largely water-soluble hydrated nitrate salts of Na, K, Ca, Mg, and Al that are bagged-out and packed in poly-lined drums. In many instances, the bags have deteriorated due to radiolysis. The residual salt samples (Table 1) from the emptied drums are essentially the 'leftovers' of the first phase of the waste drum remediation process; wherein parent drums are emptied into a glovebox, the wastes treated as required and then repackaged into separate daughter drums that are eventually transported to WIPP. The residual salts consist of discrete chunks of heterogeneous material (monolith), or aggregates of "moist, free-flowing" to "moist, clumping," macroscopically heterogeneous solids (Chamberlin and Martinez, 2014; Chamberlin et al., 2015).

While the residual salts ostensibly constitute untreated, unremediated nitrate and oxalate salts and related residues (bits of lead shielding, rust particles from the drum interior, etc.), it is possible that they have been contaminated with Swheat Scoop®. There are two possible avenues for cross-contamination with Swheat Scoop® (Schumann, 2015):

1) Wet salts from the parent drum were emptied into a glovebox at WCRRF and combined with the neutralizer and adsorbent manually, using hand tools. The same tools are also used to remove salt bags and other items from the parent drum. If hand tools were contaminated with Swheat during sorbent mixing and were then used to scoop residues out of the parent drums, cross contamination of the residues left in the drum (and later sampled for analysis) is possible.

2) During the time these drums were processed at WCRRF, it was a routine 'best management practice' to add a small amount of Swheat to an empty parent at the end of the process, before it was bagged-off, in order to ensure that any remnants of liquid in the emptied drum were completely absorbed and no longer problematic.

Table 2: MS operating parameters. Only OH, H_2O, NO, ^{36}Ar, and CO_2 were measured during every analysis

Species	*m/z*	Dwell Time (s)	Resolution	**Species**	*m/z*	Dwell Time (s)	Resolution
$(H_2)^+$	2	0.5	50	$(NO)^+$	30	0.2	50
He^+	4	0.5	50	$(O_2)^+$	32	0.05	50
C^+	12	0.5	50	$^{36}Ar^+$	36	0.05	50
O^+	16	0.2	50	$(C_3H_5)^+$	41	1.0	50
$(OH)^+$	17	0.2	50	$(CO_2)^+$	44	0.2	50
$(H_2O)^+$	18	0.2	50	$(NO_2)^+$	46	1.0	50
$(C_2H_3)^+$	27	1.0	50	$(SO)^+$	48	0.5	50
$(C_2H_5)^+$	29	1.0	50				

Table 3: DSC temperature profiles

	Preparation	**Analysis**
Profile 1	10 °C/minute ramp to 110 °C, 10 min. isotherm @ 110 °C	5 °C/minute ramp to 350 °C
Profile 2	10 °C/minute ramp to 110 °C, 10 min. isotherm @ 110 °C	2.5 °C/minute ramp to 350 °C
Profile 3	10 °C/minute ramp to 110 °C, 10 min. isotherm @ 100 °C	5 °C/minute ramp to 500 °C
Profile 4	none	10 °C/minute ramp to 1100 °C

Table 4: Calibration set 6.223.5.-91.2, RT-900 °C (for Pt-crucibles)

Material	**T_{rxn} (°C)**	**Enthalpy (J/g)**	**Purity**	**Molecular Weight (amu)**	**K =($\Delta H_{ref}/\Delta H_m$)**
$C_6H_5C_6H_5$	69.2	120.4	99%	154.21	1.040
C_6H_5COOH	122.3	147.3	>99.9%	122.12	1.096
$RbNO_3$	164.2	26.6	99.99%	147.48	1.126
$RbNO_3$	285.0	8.75	99.99%	147.48	1.142
Ag_2SO_4	426.4	51.7	99.999%	311.8	1.064
CsCl	476.0	17.2	99.999+%	168.36	1.021
K_2CrO_4	668	38.9	99.5%	194.20	0.806
$BaCO_3$	808	94.9	99.98%	197.35	0.666

Analytical Details

DSC-MS runs were performed using a Netzsch STA 409PC Luxx, operated in simultaneous TG-DSC mode. The TGA-DSC measurement head (part number 6.227.1-70+S) is designed so that thermogravimetric

(TG), differential scanning calorimetry (DSC), and evolved gas data can be collected from the same sample, simultaneously, during a single experiment. The resolution of the thermobalance is 2 μg, and the thermocouple (an integral part of the measurement head itself) is accurate to within ~0.2 °C. All data were collected and corrected for buoyancy and background effects using proprietary Netzsch "Measurement" software (v4.3.1; 17-5-2004) and processed using proprietary Netzsch "Proteus" software (v4.3.1; 17-5-2004). Onset temperatures were obtained using the 'onset' capability in Proteus. Enthalpy values were obtained by choosing a reasonable background value on either side of the peak and integrating the peak area in Proteus. Mass changes were evaluated by using the first derivative of the mass change curve (labeled "DTG" in all plots). For all energy plots, exothermic peaks point upwards.

Table 5: Thermodynamic data for phase transitions in $K(NO_3)$ from Breuer and Eysel (1982) and measured in the TGA-DSC apparatus used for this study

Transition	Onset T. (°C) literature	Onset T. (°C) measured	%RSD	DH (J/g) literature	DH (J/g) measured	%RSD
2nd order	**129**	129.5	+0.4	**-49.47**	-55.95	+13.1
melting	**334**	335.6	+0.5	**-98.35**	-94.93	-3.5
2nd order	**129**	129.0	0	**-49.47**	-55.26	+11.7
melting	**334**	335.7	+0.5	**-98.35**	-92.43	-6.0
2nd order	**129**	128.9	-0.08	**-49.47**	-56.19	+13.6
melting	**334**	335.7	+0.5	**-98.35**	-91.86	-6.6

The STA-MS is coupled to a Pfeiffer ThermoStar quadrupole MS (GSD 301T) via a 1m long heated (200 °C) silica capillary transfer line. Mass spectrometer data were acquired and processed using the Pfeiffer ThermoStar Suite (Quadstar 32-Bit, v7.03). The mass spectrometer was operated in peak hopping mode (MID), using electron ionization (EI, 70 eV). Aside from OH and H_2O, the following species were monitored for each sample: O, NO, ^{36}Ar, CO_2, and NO_2. In addition, the following species were also monitored during selected analyses: H_2, O_2, and SO. The RF polarity was normal, the ionization filament current was 1.0 mA, and the multiplier (SEM - channeltron) voltage was 1200 V during all phases of analysis. The remaining operating parameters for the GSD 301T are summarized in Table 2.
The entire apparatus (DSC and MS) is located inside a dry air glovebox fitted with hard-plumbed, filtered gas inlets and sealed electrical and telemetric feedthroughs. During analysis, ambient glovebox conditions were: temperature (T) = 27 to 32 °C, relative humidity (%RH) = 0.0 - 0.3%. Pre-run baseline values varied from approximately -6 to -5 μV.

To facilitate the thermal analysis of small (10-50 mg) quantities, the residual salt and monolith samples were dried in air at 100 °C and ground to a fine powder by C-AAC personnel. Top layer salt samples S802701 and S813389 were dried without grinding. Immediately prior to analysis, all samples were re-ground using an agate mortar and pestle. For STA-MS analysis, each nitrate and WIPP / LANL waste sample was subjected to a 10 minute-long isothermal drying interval at ~110 °C to remove reabsorbed atmospheric moisture from the samples. All relevant data was collected following the isothermal step, which served only to purge the sample of water adsorbed after the samples were first prepared by C-AAC. For all nitrate samples, and for the first round of (uncalibrated) exploratory WIPP sample runs, temperature Profile 1 was used (Table 3). Following calibration of the measurement head, Profile 2 was used in an effort to resolve the broad enthalpy peaks into discrete events which could then be related to specific chemical reactions. When that effort revealed no new data, selected WIPP samples were re-run using Profile 3. Only the calcium oxalate samples were run using Profile 4 in TGA-MS samples (no DSC data collected).

The STA was calibrated using a standard reference material (SRM) set provided by Netzsch (6.223.5-91.2), which consists of the materials listed in Table 4. These materials were used to construct calibration curves for the measurement of temperature and enthalpy using the TGA-DSC measurement head. K-values, the ratio of the reference enthalpy values to those measured in our apparatus ($\Delta H_{ref}/\Delta H_m$), for each standard are also listed in Table 4. A KNO_3 sample (25.53 mg) was run in triplicate (Table 5) to evaluate the precision and accuracy of the onset temperatures and ΔH measurements relative to literature values (Breuer and Eysel, 1982). Onset temperatures vary from known literature values by <1.0%, while the enthalpy measurements (obtained by integrating the peak area using Netzsch Proteus software) vary from the values in Breuer and Eysel (1982) by ~+7% to ~-14%.

Table 6: Summary of XRD phase identification results (major phases in S855793 in bold text), total Pu, volatiles (mass loss after the as-received solid was heated in air for 15 hrs. at 200 °C), combustibles (additional mass loss after the 200 °C material was heated in air for an additional 1 hr. at 600 °C), and calculated non-nitrate combustible content from Martinez et al., 2015; Chamberlin and Martinez, 2014, and Chamberlin, et al 2015.

Sample	Origin	Phases detected by XRD	Total Pu (µg/g)	Wt. % Volatiles	Wt. % Combustible (total)	Wt. % Combustible (non-nitrate)
S802701	S802701	$NaNO_3$	14	11.8 *(LOI to 110 °C)*	n.a.	n.a.
S813389	S813389	$NaNO_3$, $Mg(NO_3)_2$	60	24.5 *(LOI to 110 °C)*	n.a.	n.a.
69139	S864694	amorphous, $Pb(NO_3)_2$, $NaNO_3$	496	18.7	46.1	27.8
68492	S822952	amorphous, $Pb(NO_3)_2$, $NaNO_3$	83	20.6	57.3	38.6
68645	S818449	amorphous, $Pb(NO_3)_2$, $NaNO_3$	96	37.3	27.9	11.6
69173	S851436	amorphous, $PbCO_3$, $Pb(NO_3)_2$, $NaNO_3$	41	14.4	35.3	22.8
69120-1	S855793	**$NaNO_3$, $Pb(NO_3)_2$**, amorphous, $Pb_2(NO_3)_2(C_2O_4)$, PbO_2	394	6.92 *(LOI to 110 °C)*	n.a.	n.a.
69120-2	S855793	**$NaNO_2$, $PbCO_3$**, amorphous, $NaNO_3$, Na_3ONO_2, $MgCO_3$, $Pb(NO_3)_2$, Pb_2OCO_3	33	2.15 *(LOI to 110 °C)*	n.a.	n.a.
69120-3	S855793	**$NaNO_3$, $Pb(NO_3)_2$**, amorphous, PbO_2, $Pb_2(NO_3)_2(C_2O_4)$	262	25.65 *(LOI to 110 °C)*	~32.8 (110-600 °C)	n.a.

The sample outgas is entrained in a ~80 mL/min ultra-high-purity (UHP) Ar flow. Although the TGA furnace and gas inlets were evacuated and flushed with UHP Ar prior to sample loading, some air was admitted to the sample chamber when it was opened to load the sample. At the beginning of each analysis, the Ar content of the headspace was between 10 to 40%, with the balance as dry air. During analysis, Ar content steadily increased to 40-70%. Samples were transferred using a spatula into a clean platinum-rhodium (Pt-Rh) STA pan, placed on the DSC carrier and covered with a pierced Pt-Rh lid. The reference pan was an empty Pt-Rh pan-and-lid assembly.

Figure 1: DSC-MS data for sodium nitrate to 350 °C

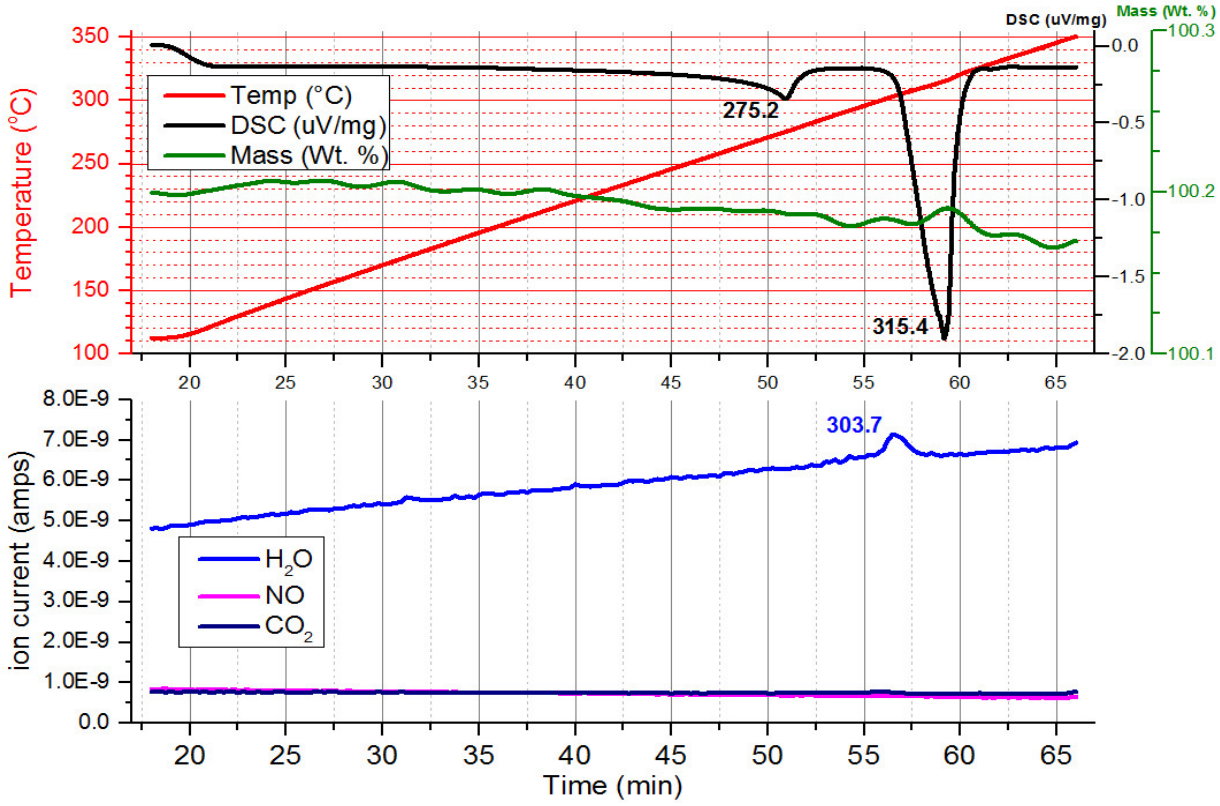

Results

Pure Nitrates and Oxalate

The XRD data reported by Martinez, et al. (2015), Drake (2014), and Chamberlin, et al (2015) indicate that both $Pb(NO_3)_2$ and $NaNO_3$ are major components of the drum residues, along with varying amounts of amorphous material and an array of other constituents, including Pb mixed salts and sodium nitrite(Table 6). In order to evaluate the response of parent drum samples, we analyzed selected nitrates and nitrate hydrates. DSC results from these samples were in broad agreement with those from published work.

Calcium oxalate hydrate samples (0.60 to 11.58 mg) were previously run in 2013 using Profile 4 in TGA-MS mode (i.e., no DSC data). We identified three distinct mass loss events. The first, occurring between 130 and 167 °C is a simple dehydration, resulting in mass losses of -12.0 to 16.2 wt. %. Two separate decarbonation reactions occur at 463.0 to 471.8 °C (CO_2 + CO: mass loss: -18.8 to -25.3 wt. %) and 652.2 to 735.5 °C (CO_2 only: -29.7 to -34.7 wt. %).

All nitrate and nitrate hydrate samples were run in STA-MS mode. One of the primary constituents of the WIPP and LANL drum samples is $Na(NO_3)$ which, as a pure phase, shows no mass change, but did show two significant endothermic reactions (Bauer et al., 2009) below 350 °C: a second order phase transition at 275.2 °C, and melting at 315.4 °C (Figure 1). A small amount of H_2O is evolved during melting. The other major nitrate constituent, $Pb(NO_3)_2$, shows no reactivity or mass change whatsoever below 350 °C, with just minor evolution of NO at ~300 °C.

Figure 2: DSC-MS data from $Mg(NO_3)_2 \cdot 6H_2O$ using Profile 1. Regions A, B, and C correspond to different furnace programming segments (see Table 3).

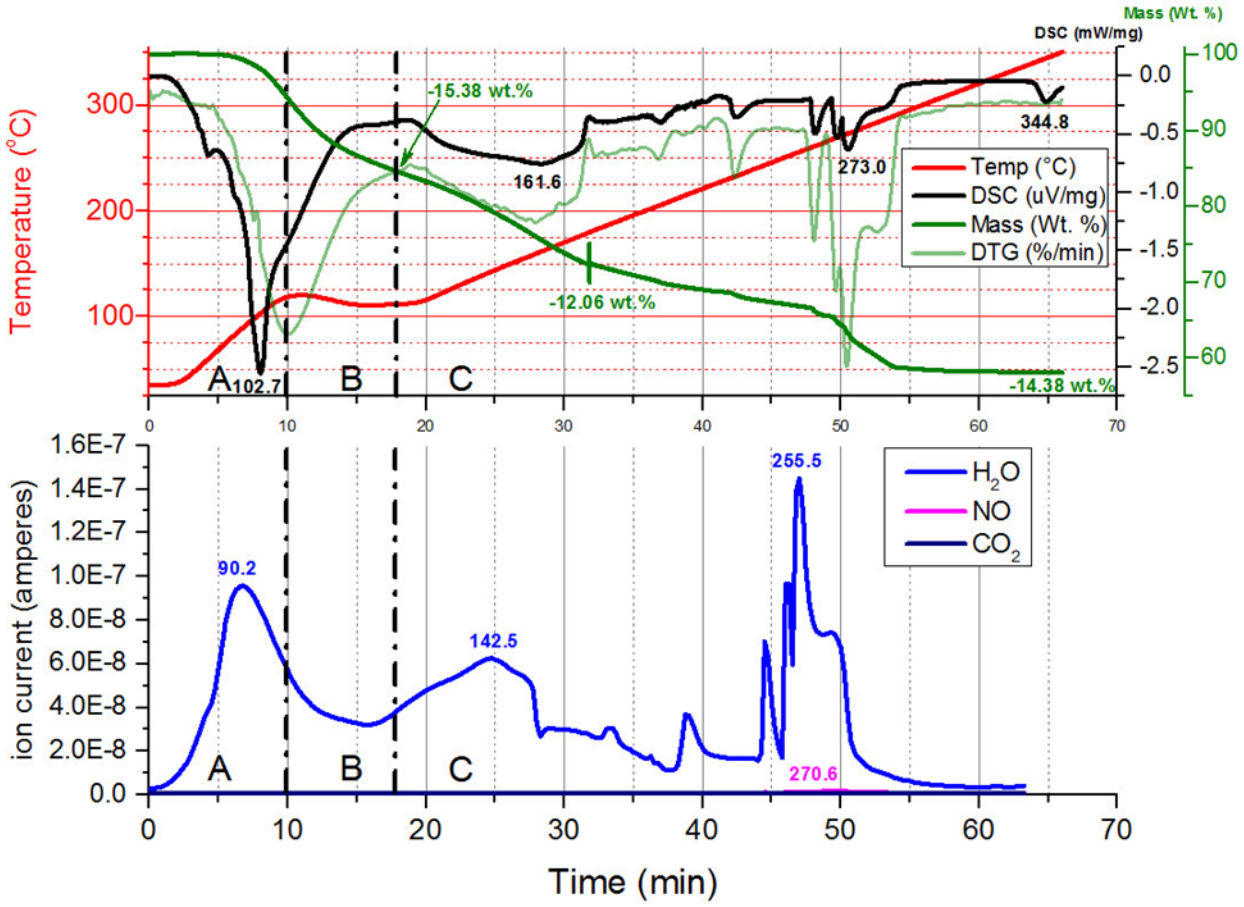

Similarly, $K(NO_3)$, a possible minor constituent of the nitrate salt fraction, shows no mass change and two significant endothermic peaks at 136.8 °C and 341.5 °C, each associated with barely detectable releases of H_2O and CO_2 below 350 °C. Magnesium nitrate hexahydrate, $Mg(NO_3)_2 \cdot 6H_2O$, dehydrates in three distinct stages (Figure 2) with onset temperatures of 42.5, 112.8 and 259.9 °C. Water derived from these endothermic dehydration reactions dominates the gas releases up to 350 °C. The total mass change was -26.4 wt. %.

The only trivalent nitrate salt examined as part of our preliminary study was ferric nitrate hydrate, $Fe(NO_3)_3 \cdot 9H_2O$. Iron (III) nitrate hydrate released significant H_2O and NO_x during the initial part of the isothermal drying step, and therefore was re-run in STA-MS mode using Profile 4 to 400 °C, without the isothermal drying step. Also thought to be a constituent of the nitrate fraction in both the LANL and WIPP drums, iron (III) nitrate was also the only compound to react to a different end-product and the only one that released significant amounts of H_2O and NO_x below 350 °C (Figure 3).

Results from $Fe(NO_3)_3 \cdot 9H_2O$ are similar to those obtained by previous workers (ElMasry et al, 1998; Wieczorek-Ciurowa and Kozak, 1999). When heated to 500 °C at 10 °C/min, dehydration onsets at ~46 °C, while the release of NO begins at ~110 °C. The H_2O peak reaches a maximum value between ~140 and 165 °C. The emission of NO, NO_2, and CO_2 reach a maximum simultaneously, at ~162-168 °C.

Dehydration and denitrification appear to be largely endothermic in nature, though within the overall endothermic trend one or several smaller exothermic peaks appear at ~79-88 °C, ~135-143 °C, and ~163 °C. The endotherm peaks at ~167 °C, almost simultaneously with the maximum NO / NO_2 / CO_2 gas release. The total mass lost up to 400 °C was ~71 to 76 wt. %. In each case, an insoluble reddish-brown to black residue remained, presumably comprised of Fe oxides or oxyhydroxides (e.g., Gadalla and Yu, 1990; Wieczorek-Ciurowa and Kozak, 1999).

Figure 3: DSC-MS data (to 410 °C) from Fe(III) nitrate hydrate.

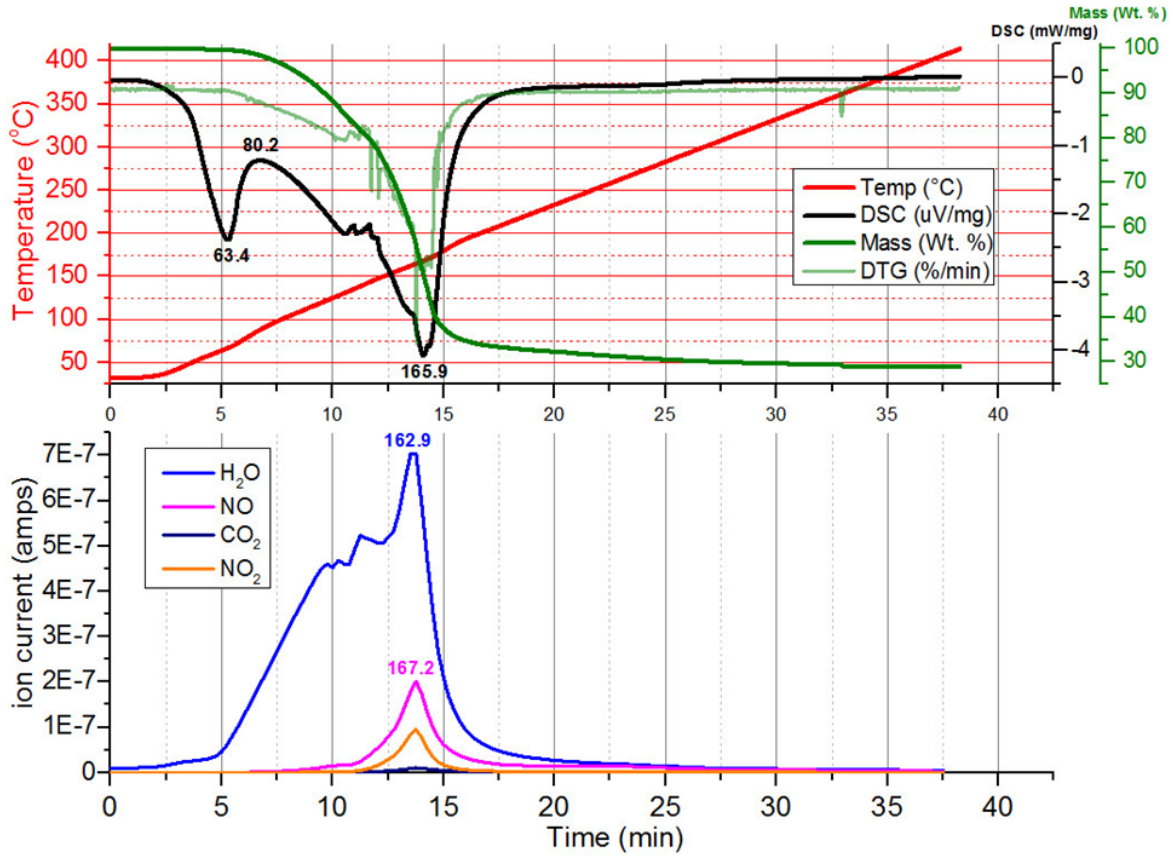

LANL Parent Drum Samples

Top Layer Salts

When analyzed by DSC-MS using Profile 1 (Figure 4), the salt sample from the top layer of S802701 behaved identically to pure $Na(NO_3)$. This sample was not analyzed further. A similar sample, S813389, which contained greater amounts of $Mg(NO_3)_2{\cdot}6H_2O$ (Drake 2014), was analyzed using Profile 4 (Figure 5). DSC-MS data from S813389 do not resemble those from S802701, despite its Na content (~8.5 wt. %). The thermal behavior of this sample somewhat resembles that of Mg nitrate hexahydrate, except that dehydration is complete in a single event. S813389 loses mass in 3 discrete steps: endothermic dehydration (-7.15 wt. %), which onsets at 92.0 °C and peaks at 111.1 °C (though H_2O emission reaches a maximum at 195.5 °C); incipient de-nitrification (-3.72 wt. %) from 316–394 °C, and denitrification (-25.19 wt. %) which starts at ~395 °C and continues to the end of the run. The second de-nitrification reaction was not complete when the run was terminated at 500 °C.

Figure 4: Comparison of DSC data from pure reagent grade $Na(NO_3)$ [top], and Sample S802701 [bottom].

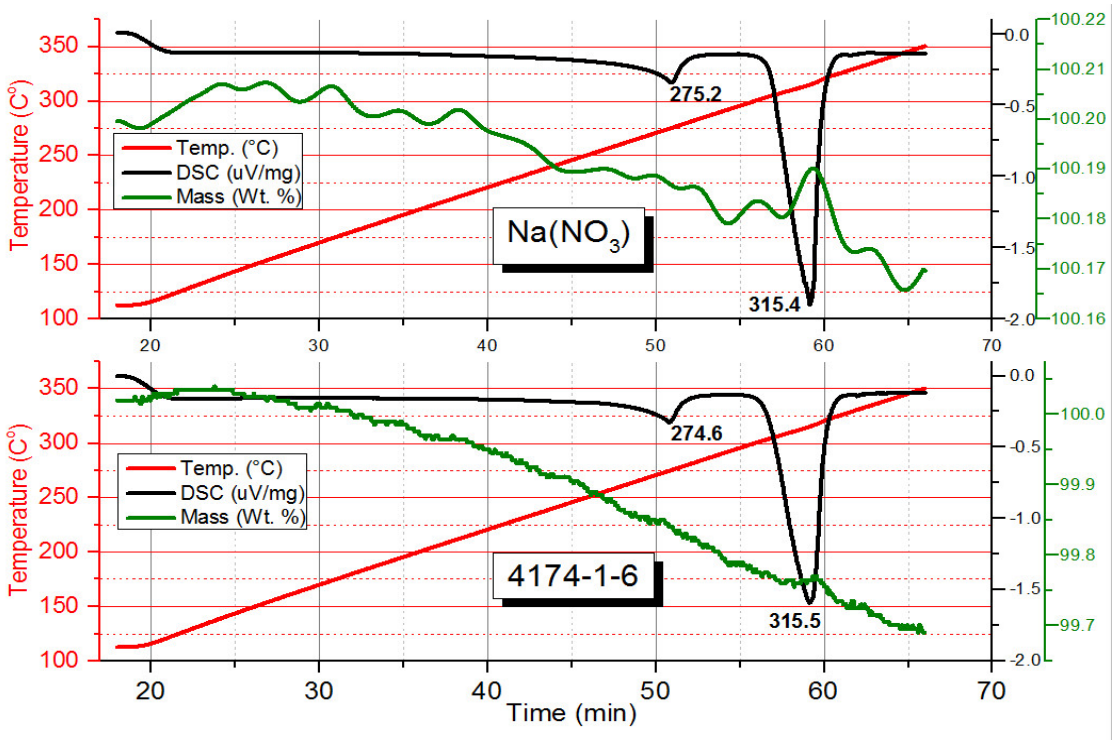

Residual Salts

68492 – S822592: Analyzed using Profile 3 to 500 °C, this sample (Figure 6) lost 43.45 wt. % in two overlapping stages: -27.42 wt. % from 100 °C to 304.2 °C and an additional -16.03 wt. % from 304.2 °C to 500 °C. Both mass loss events were accompanied by gas releases and overlapping exothermic reactions. The first reaction onsets between 217.0 and 227.0 °C and quickly rises to an energy peak at 254.6 °C. This reaction corresponds to a dehydration event with concomitant lesser and approximately equal releases of NO and CO_2. The second reaction maximized at 342.6 °C and was accompanied by further release of CO_2 and NO, with little or no further dehydration. As the run ended, beginning at ~430 °C, a third broadly exothermic reaction initiates and is associated with further CO_2 release. An interesting characteristic of this sample is the small endothermic peak at 131.2 °C, likely a second-order phase transition in one of the solid constituents.

68645 – S818449: Between 100 °C and 500 °C, this sample (Figure 7) lost a total of 46.51 wt. % in three overlapping stages: -9.31 wt. % from 100 °C to 248.2 °C, -13.43 wt. % from 248.2 °C to 321.2 °C, and an additional 23.77 wt. % from 321.2 °C to 500 °C. Each of these mass losses bound corresponding, overlapping exothermic reactions and gas release events. Onset of the first reaction occurs between 160.4 and 174.4 °C and reaches a maximum at ~216.3 °C. The product of this reaction is primarily H_2O vapor. The second reaction onsets at ~240.2 °C, peaks at 305.0 °C, and releases both NO and CO_2. The H_2O from the previous reaction is still being released at this time. The third reaction onsets at ~348.0 °C and rises quite rapidly to a maximum at 365.5 °C. This reaction generates substantial amounts of NO and CO_2. A final dehydration produces a water peak at 377.8 °C, with little impact on the mass change curve.

69173 – S851436: Analyzed using Profile 3 to 500 °C, this sample (Figure 8) lost 44.46 wt. % in two stages: -19.78 wt. % from 100 °C to 271.7 °C and an additional -24.68 wt. % from 271.7 °C to 500 °C. The

first mass loss was accompanied by a very large H_2O peak (255.1 °C), with subordinate and simultaneous releases of NO and CO_2. A significant exotherm (onset temperature = 204.8 °C; peak @ 257.7 °C) occurs simultaneously with the de-gassing reaction. Subsequent mass loss is more or less continuous. Small CO_2 emissions occur at 304.4 °C and 396.2 °C, and coincide with minor endothermic peaks at 302.4 °C and 399.2 °C. Both also coincide with small mass loss events, as indicated by the DTG curve in Figure 8.

Figure 5: DSC-MS data from the top layer salt sample S813389.

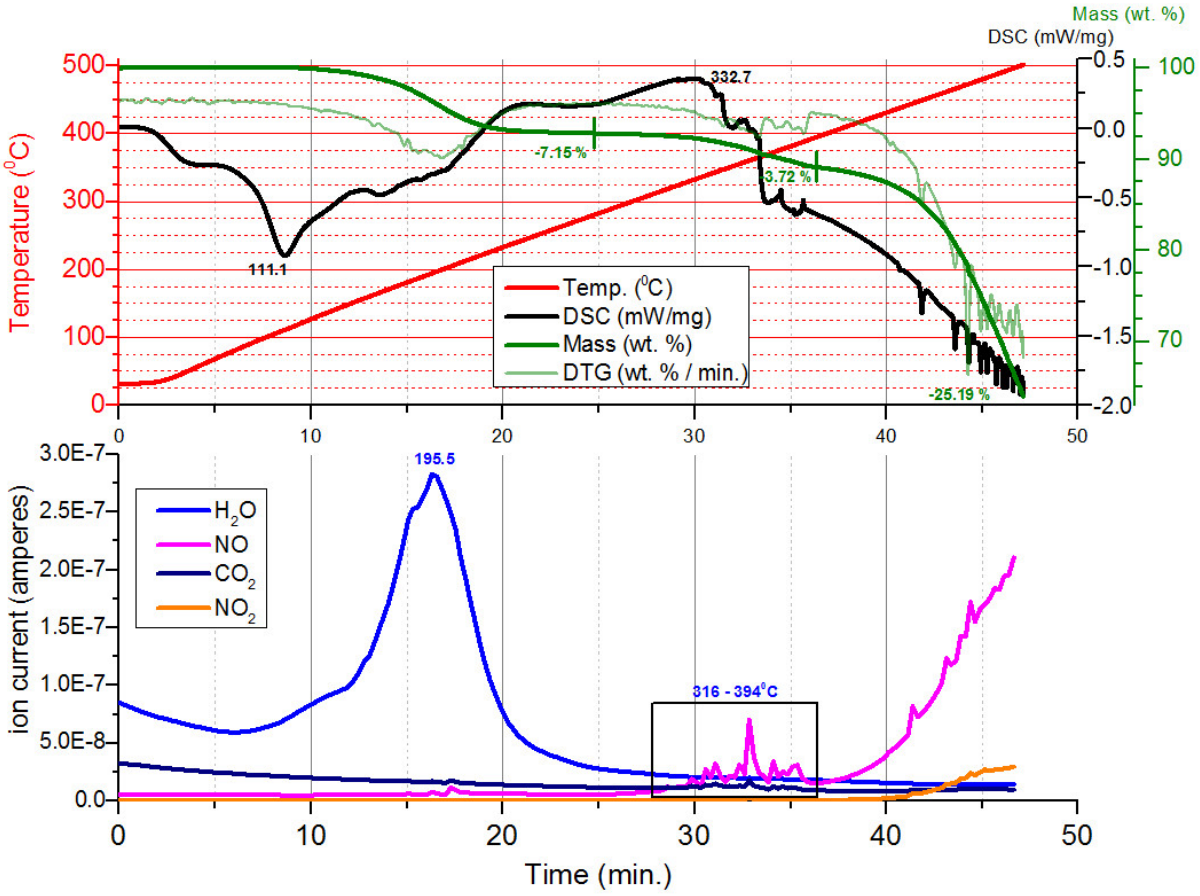

<u>69139 – S864694</u>: Between 100 and 500 °C, this sample (Figure 9) lost a total of 34.56 wt. % in four identifiable stages: -13.33 wt. % from 100 to 280.1 °C, -10.38 wt. % from 280.1 to 336.6 °C, -7.99 wt. % between 336.6 to 473.9 °C and an additional 2.86 wt. % from 473.9 °C to the termination of the run at 500 °C. Each of these mass losses bound corresponding, overlapping exothermic reactions and gas release events. Onset of the first and most exothermic reaction occurs between 223.6 and 234.1 °C and reaches a maximum at 253.2 °C. The product of this reaction is primarily H_2O vapor, with lesser amounts of NO and CO_2. The second reaction onsets at ~293.6 °C, peaks at 309.8 °C and releases mostly CO_2 with lesser amounts of NO and little or no H_2O. The third reaction shows a broad exotherm at ~348.1 °C with coeval releases of CO_2 and NO. The mass loss between 473.9 °C to the termination of the run at 500 °C doesn't correspond to a reaction, but is accompanied by NO emission that peaks at 473.9 °C.

Figure 6: DSC-MS data (to 500 °C) for residual salts from LANL parent drum S822952, sample 68492.

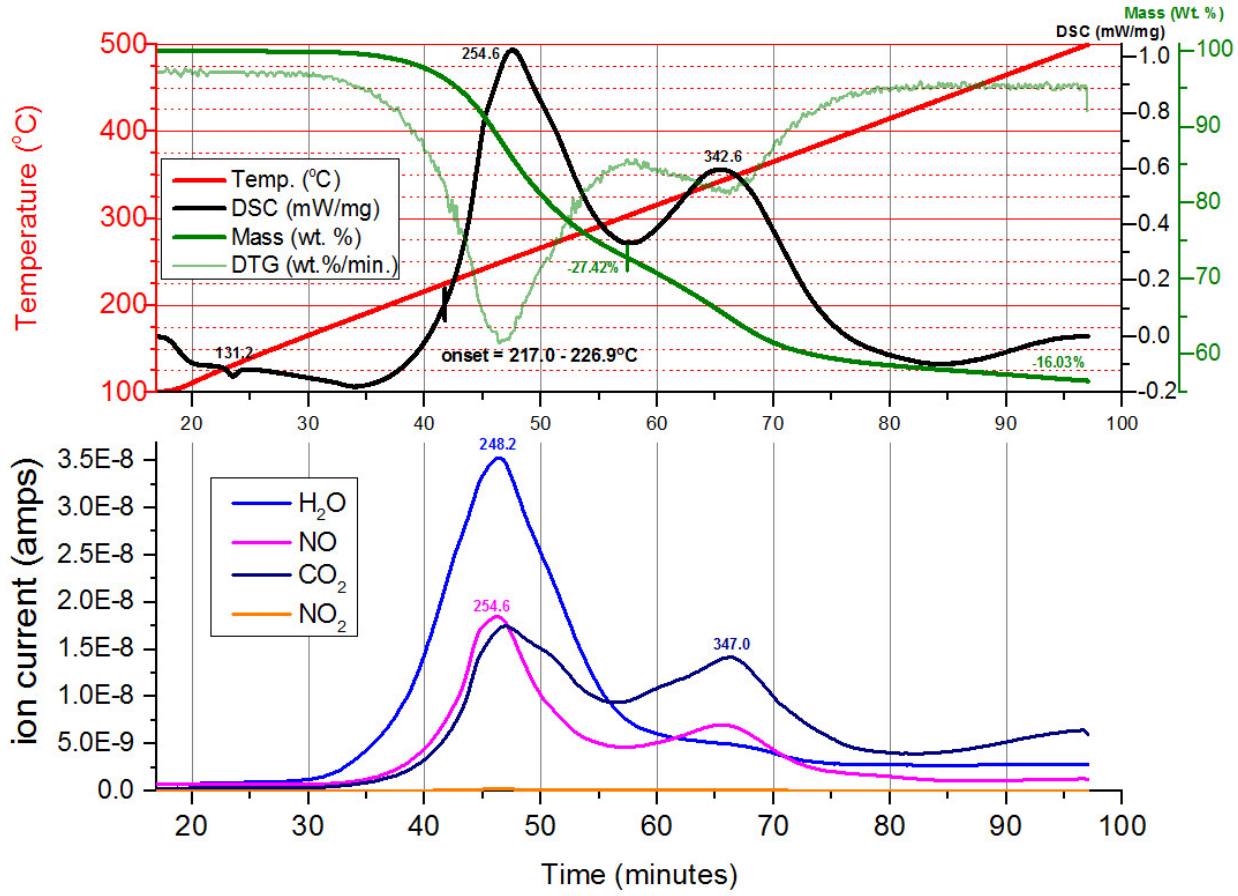

Monolith Samples from LANL Parent Drum S855793

Each of these samples is different, macroscopically (Figure 10), and each has a different mineralogy as shown by X-Ray diffraction results (Martinez, et al., 2015; and Table 6). We performed a preliminary analysis on each sample using Profile 1 (Table 3), and then each sample was re-analyzed using Profile 4. Results from both analyses are consistent, though only the results to 500 °C (Profile 4) are discussed here. Mass loss data does not include the loss of hygroscopic water sorbed during the interval between sample preparation and analysis. After analysis to 500 °C, the residue was a crusty, red-brown powder that resembles ground nutmeg in appearance. The red-brown color of the residue suggests the presence of either red lead oxide (PbO) or Fe^{3+} oxides and oxyhydroxides.

Monolith Sample 1 – 69120-1: XRD identified four phases in this sample. Of the four, $NaNO_3$ and $Pb(NO_3)_2$ are the most abundant, while smaller quantities of $Pb_2(NO_3)_2(C_2O_4)$ and PbO_2 can be inferred from the relative intensities of the XRD peaks. In addition, XRD analysis indicates that there is a sizable amorphous component in this sample (Martinez, et al., 2015). The DSC results are quite complicated (Figure 11), and the determination of onset temperatures is, in most cases, complicated by overlapping reactions. The data show at least three exothermic peaks at 194.2 °C, 238.3 °C, and 303.6 °C, and at least three endothermic peaks at 150.5 °C, 263.6 °C, 365.9 °C. The last of these endothermic reactions has an onset temperature of ~355.0 °C. A final endotherm onsets at ~451 °C and has not reacted to completion by the end of the run at 500 °C. The mass change curve is similarly complex, with up to 5 distinct mass

loss events between 100 °C and 500 °C. The total mass loss from the 38.98 mg sample was -26.11%, significantly less than observed from the other samples.

Figure 7: DSC-MS data (to 500 °C) for salt residue LANL parent drum S818449, sample 68645.

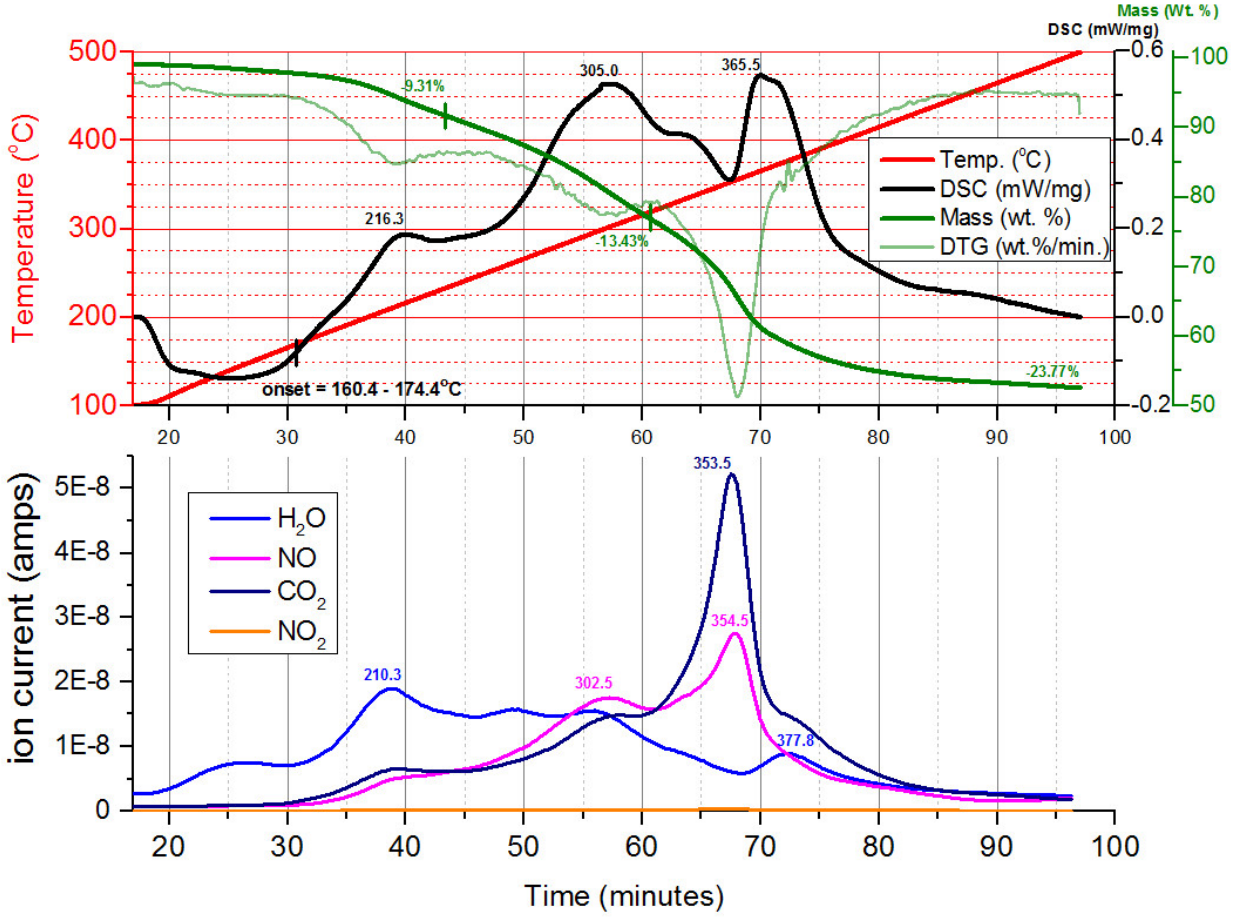

The first mass loss, -2.43%, occurs between 100 °C and 262.6 °C and corresponds to dehydration (H_2O peak at 232.3 °C). An endotherm and two exothermic peaks occur in the region, followed by an endotherm that also peaks at 262.6 °C. Between 262.6 °C and 316.3 °C, the sample loses an additional 14.04 wt. %, exothermically (303.6 °C) accompanied by the evolution of a large amount of CO_2, NO, and NO_2. Very little to no water is lost during this step, nor is any evolved during any of the subsequent gas-release events. The next mass loss, 3.64 wt. %, occurs between 316.3 °C and 347.0 °C and corresponds to a shoulder in the DSC curve and a discrete pulse of CO_2 (330.2 °C) and NO (324.7 °C). An additional decarbonation occurs between 347.0 °C and 398.2 °C (CO_2 peak at 363.4 °C) is endothermic (peak at 365.9 °C), and results in a mass loss of 2.17 wt. %. A final mass loss (-3.83 wt. %) corresponds to the endothermic trend which onsets at ~451.0 °C and continues through the end of the run. This reaction is coeval with the release of large amounts of NO and NO_2.

Monolith Sample 2 – 69120-2: Cerussite ($PbCO_3$), sodium nitrite ($NaNO_2$), and amorphous material are the primary constituents of this sample, with minor amounts of $NaNO_3$, $Pb(NO_3)_2$, shannonite ($Pb_2O(CO_3)$), sodium nitrate oxide ($Na_3O(NO_2)$), and magnesite ($Mg(CO_3)$). The DSC-MS results (Figure 12) from this sample are, again, quite complicated and consist of a succession of moderate endo- and

exothermic reactions, multiple mass loss steps, and multiple gas evolution events. Over the 100 °C to 500 °C temperature interval, 69120-2 released less gas and lost less mass (total = -19.76 wt. % of 41.28 mg) than 69120-1. Endothermic reactions on the DSC curve (i.e., pointing downwards) correspond to four of the five significant gas releases from the sample; the first onsetting at ~157.3 °C. The mass loss curve shows at least five discrete steps at 201.1 °C, 262.1 °C, 331.1 °C, 380.3 °C, and 452.9 °C.

Figure 8: DSC-MS data (to 500 °C) for residual salt from LANL parent drum S851436, sample 69173

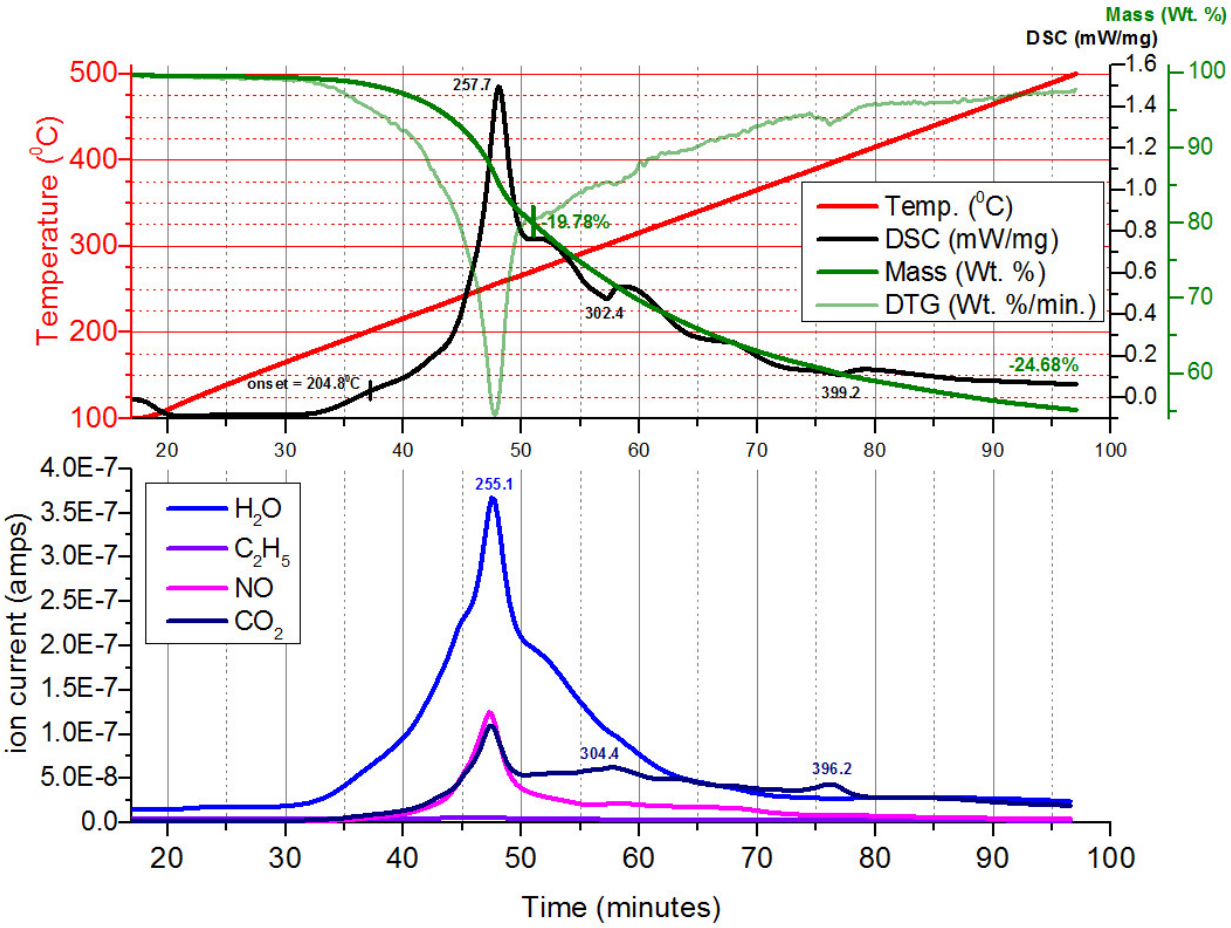

The first mass loss, -1.42 wt. %, occurs between 100 °C and 201.1 °C and corresponds to endothermic (184.3 °C) dehydration (H_2O peak at 184.8 °C). A second mass loss event (-2.90 wt. %) occurs between 201.1 °C and 262.1 °C, and may be related to the first of three decarbonation events, at 233.1 °C. Decarbonation terminates in the vicinity of an exothermic reaction which onsets at 234.6 °C and peaks at 261.6 °C. The largest magnitude mass loss, -6.09 wt. %, occurs between 262.1 °C and 331.1 °C, and corresponds to the endothermic (307.2 °C) release of CO_2 and a minor amount of NO at 305.7 °C. The next mass loss, between 331.1 °C and 380.3 °C corresponds to a third CO_2 release (endothermic reaction onsetting at 340.5 °C and peaking at 347.5 °C), this time not accompanied by significant NO. The last two mass loss events, between 380.3 °C and 452.9 °C, and from 452.9 °C to the end of the run, correspond to NO releases at 432.5 °C, and 495.6 °C. Both of these de-nitrification reactions seem to be related to endotherms that peak at 435.9 °C and 495.6 °C. The latter reaction onset occurs at 467.8 °C.

Figure 9: DSC-MS data (to 500 °C) for residual salt from LANL parent drum S864694, sample 69139

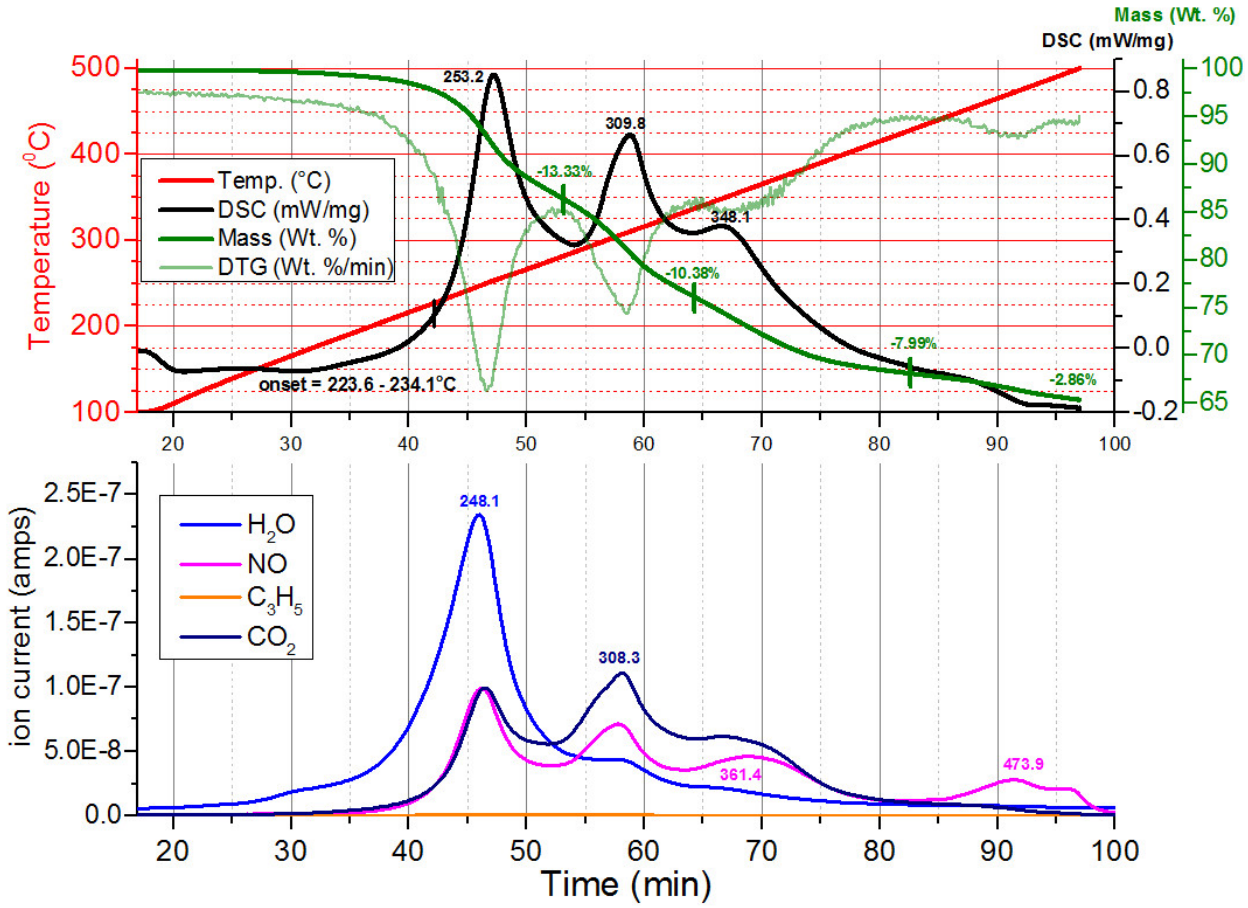

Figure 9: Residual salt monoliths from parent drum S855793, sample 69120. See Table 7 for explanation

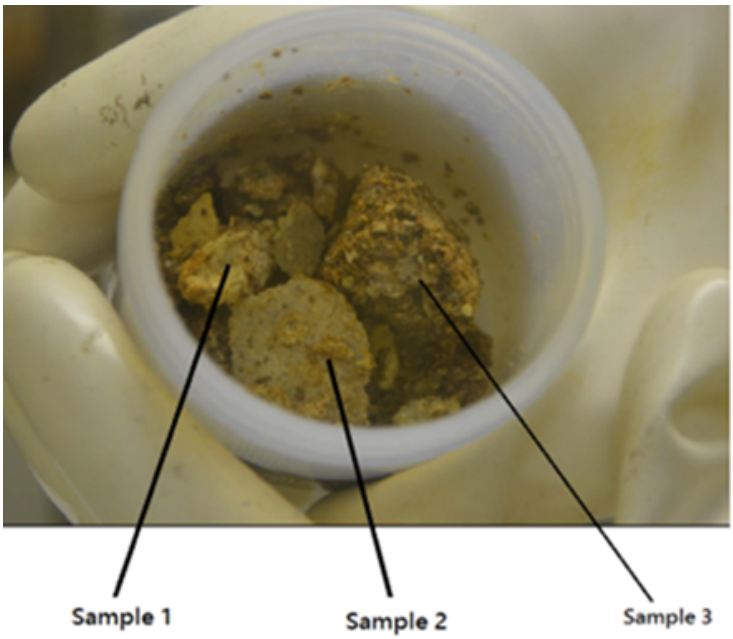

Figure 10: DSC-MS data (to 500 °C) for residual salt from LANL parent drum S855793, sample 69120-1 (#1). Peak temperatures in bold text, onset temperatures are in regular text.

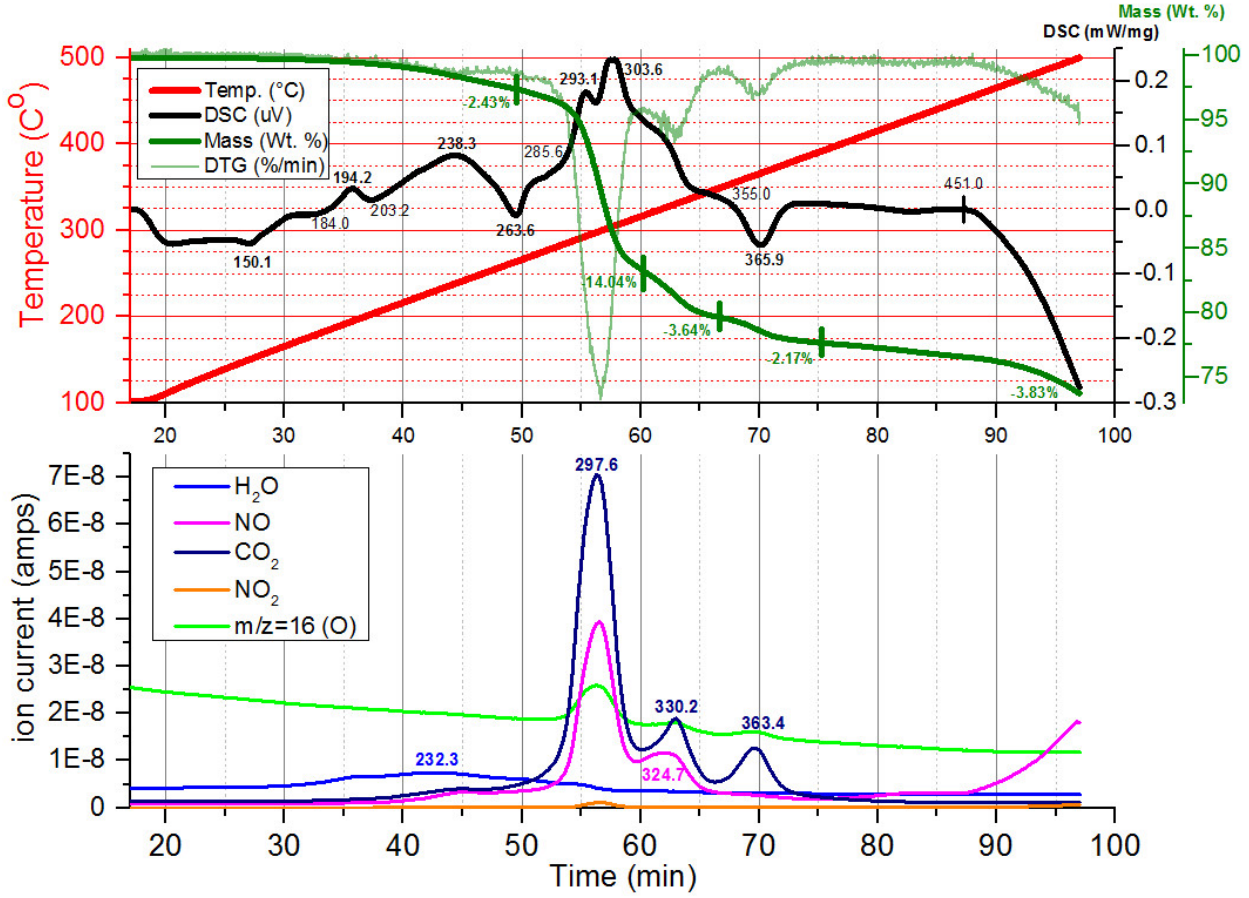

Monolith Sample 3 – 69120-3: XRD results (Martinez et al., 2015 and Table 6) indicate that 69120-3 has a similar mineralogy to 69120-1. However, DSC-MS analysis indicates that this sample's thermal and gas generation behavior between 100 °C to 500 °C is very distinct from that of 69120-1 and 69120-2. The DSC-MS results (Figure 13) from this sample are less complex than observed for 69120-1 and 69120-2, with only two large exothermic energy maxima. The mass loss and gas release spectra, however, are very complex and indicate multiple, coeval mass loss steps and gas evolution events with increasing temperature. From 100 °C to 500 °C, 69120-3 released far more gas and lost the most mass (total = -40.35 wt. % of 29.66 mg) of the three salt residue samples from S855793. Unlike 69120-1 and 69120-2, the two major exothermic reactions on the DSC curve (i.e., pointing upwards) correspond directly to the two major gas release events from the sample. No endothermic reactions were observed over the 100 °C to 500 °C analysis interval. The mass loss curve shows four discrete steps, from 100 °C to 283.3 °C, from 283.3 °C to 333.2 °C, from 333.2 °C to 422.0 °C, and from 422.0 °C to the end of the run.

Figure 11: DSC-MS data (to 500 °C) for residual salt from LANL parent drum S855793, sample 69120-2 (#2)

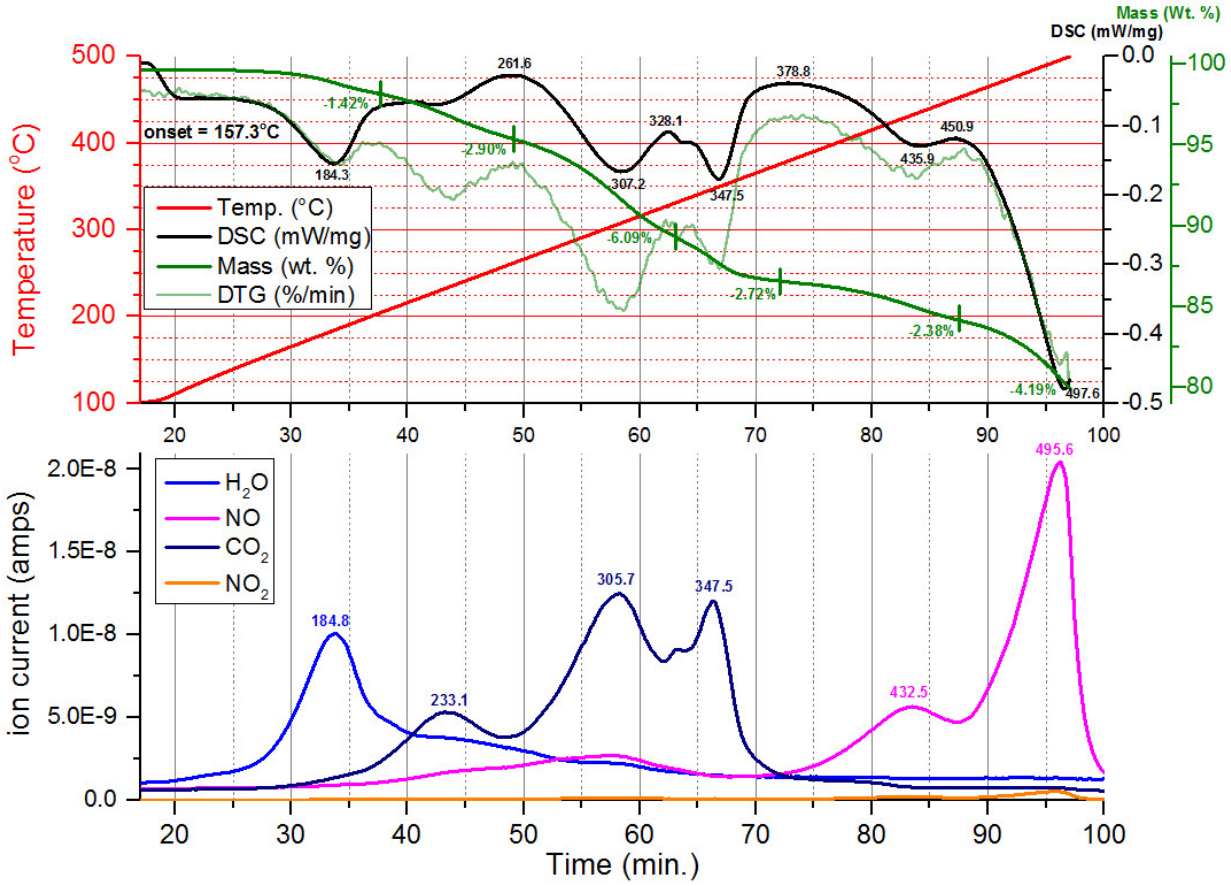

The first mass loss, between 100 °C to 283.3 °C (-19.66%) corresponds to a highly exothermic reaction which onsets between 161.7 and 166.6 °C, and peaks at 251.4 °C with a simultaneous release of copious amounts of H_2O (248.4 °C), CO_2 and NO / NO_2. The second large exothermic peak onsets at ~296.3 °C and peaks at 319.0 °C, though both the 1st derivative of the mass change curve (DTG on Figure 12) and the gas abundance data suggest that the second peak is comprised of two discrete mass change events. Between 283.3 °C and 333.2 °C, mass changes by -10.57%. The gas released is predominantly CO_2 (maximum at 309.0 °C) with lesser amounts of H_2O. As this reaction winds down, a new reaction occurs resulting in additional mass loss (-8.06 wt. %) between 333.2 °C and 422.0 °C, and liberating additional CO_2 (maximum at 341.6 °C) and NO (maximum at 348.0 °C). This reaction is also exothermic, but produces only a shoulder on the high-temperature side of the peak at 309.0 °C. To the end of the run, at 500.0 °C, further mass loss (-2.06 wt. %) is associated with the release of a small amount of CO_2.

Figure 12: DSC-MS data (to 500 °C) for residual salt from LANL parent drum S855793, sample 69120-3 (#3).

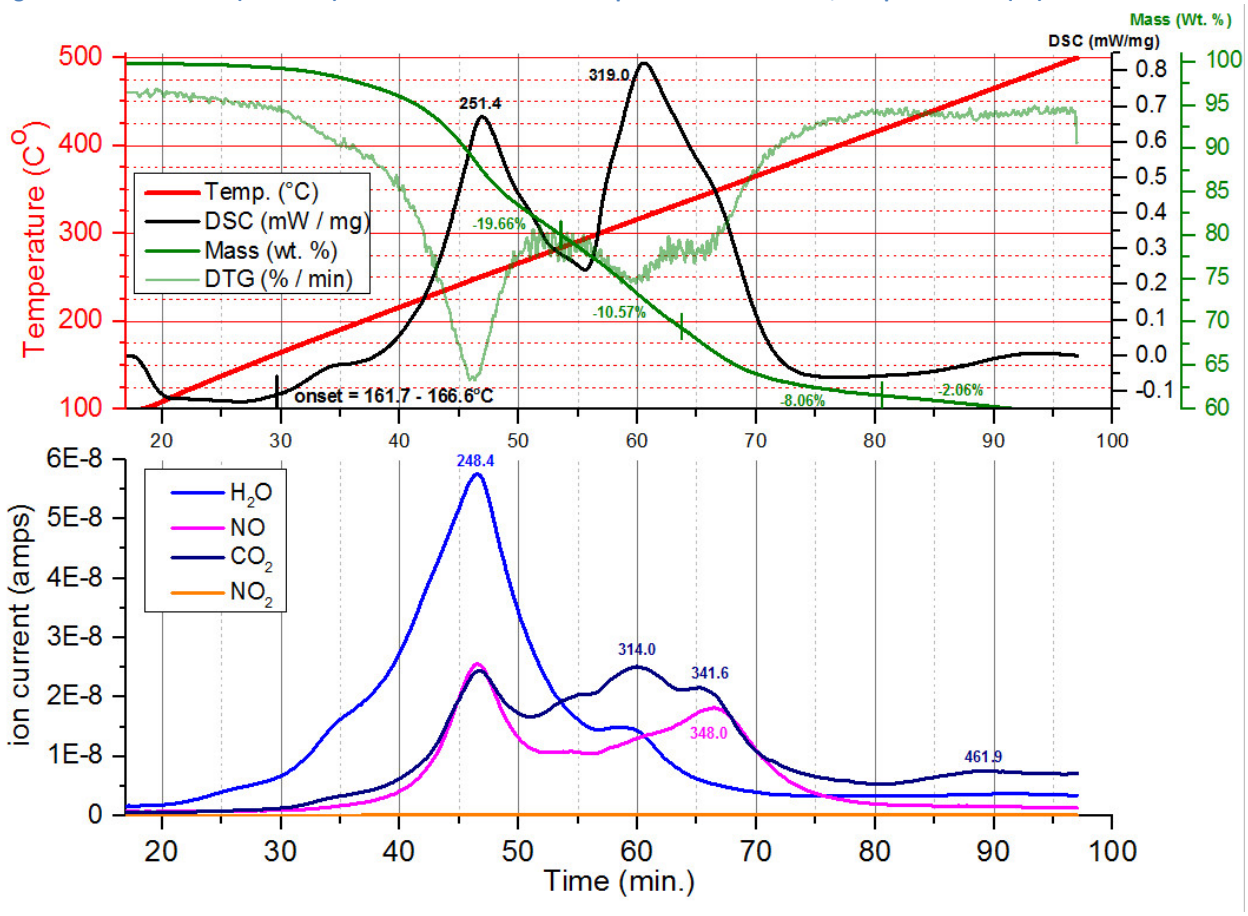

Discussion

Pure Nitrates vs. LANL Top Layer samples

Thermal analyses of pure Na, K, and Pb nitrates and the nitrate hydrates of Mg and Fe^{3+} revealed little in the way of reactions or potentially dangerous gas releases below 350 °C. Lead nitrate showed little reaction of any kind, while anhydrous $K(NO_3)$ and $Na(NO_3)$ undergo mild endothermic reactions which correspond to second order crystallographic transitions, followed by melting. As expected, the hydrous nitrates of Mg and Fe^{3+} respond quite differently. From room temperature to 350 °C, magnesium nitrate hexahydrate (Figure 13) dehydrates endothermically, starting well below 100 °C, in several discrete stages, eventually losing ~42 wt. % of its mass. A trace amount of NO is evolved at ~270.6 °C. Dehydration of $Fe(NO_3)_3{\cdot}9H_2O$ (Figure 2) onsets at ~46 °C, and the sample begins to de-gas NO^+ and NO_2^+ at ~110 °C. The H_2O peak reaches a maximum value between ~140 and 165 °C, while NO and NO_2 emissions reach a maximum simultaneously, at ~162-168 °C. Both reactions are largely endothermic in nature. No further reactions occur above ~200 °C, as the sample has reacted completely to a red-brown residue, likely Fe_2O_3 or a mixture of Fe^{3+} oxides and oxyhydroxides (Gadalla and Yu, 1990; Wieczorek-Ciurowa and Kozak, 1999), with a total mass loss of ~71 to 76 wt. %.

Top layer salts consist largely of Na and Mg nitrates. The DSC-MS data (Table 7) from one of the top layer salt samples, S802701 are identical to those obtained from pure $NaNO_3$ (Figure 3). This sample was completely soluble in H_2O and in 2% HNO_3, and its trace and minor constituents include 10s to >1000

mg/g of K, Fe, Ca, Pb, Mg, Ni, and Cr (Chamberlin and Martinez, 2014; Chamberlin et al, 2015). The radioactive element contents of this sample are relatively low: ^{235}U = 1600 μg/g; ^{238}U = 840 μg/g; and 1 μg/g or less of ^{239}Pu, ^{237}Np, and ^{241}Am (Chamberlin and Martinez, 2014; Chamberlin et al, 2015). Impurities of these elements at these levels appear to have no effect on the sample's thermal characteristics.

The other top layer salt sample, S813389, appears to be a hydrous mixture of Na and Mg nitrates with trace amounts (e.g., 10s to 100s of μg/g) of Al, K, Ca, Fe, and Ni (Chamberlin and Martinez, 2015) but only 9 μg/g of ^{238}U. Investigators noted the presence of brown flecks in the residue remaining after digestion in 2% HNO_3 (Chamberlin and Martinez, 2014; Chamberlin et al, 2015). XRF analyses of the residues revealed measurable quantities of several first-row transition elements, plus Si, Ca, Ba, Ta, W, Pb, and Pu (Chamberlin and Martinez, 2014; Chamberlin et al, 2015; Martinez et al., 2015). Heated to 500 °C (Figure 4) the sample dehydrates, emitting a single large pulse of H_2O (max. temp = 195.5 °C) followed by 'spiky' discharges of NO and NO_2 between 314 and 395 °C, possibly indicative of melting. Above 395 °C, the sample begins to break down completely, emitting copious amounts of gaseous NO and NO_2.

Though it is a mixture of Mg and Na nitrates, DSC-MS data from S813389 resembles neither those of pure $Mg(NO_3)_2 \cdot 6H_2O$ (Figure 2), nor pure $Na(NO_3)$. Like Fe nitrate hydrate, S813389 exhibits a single dehydration event above 100 °C. However, the concomitant losses of NO and NO_2 at low temperature seen in Fe nitrate hydrate are not seen in S813389. Instead, gaseous NO and NO_2 is liberated independently, at much higher temperatures. The energy flow during each of these reactions is largely endothermic. We observed only minor NO evolution from pure Mg nitrate hydrate up to 350 °C (Figure 13). However, the experimental results of Mu and Perlmutter (1982) indicate that anhydrous $Mg(NO_3)_2$ begins to denitrify above ~300 °C. Though there is no data in the literature on the thermal behavior and phase stability of mixed Na and Mg nitrate salts, Reddy et al. (2012) documented the formation of a hybrid potassium nitrate–magnesium nitrate compound, $[2KNO_3 \cdot Mg(NO_3)_2]$, with unique thermal characteristics. It is possible that analogous compounds may also occur on the $NaNO_3$ - $Mg(NO_3)_2$ join.

Residual Salt Samples

Samples 68645, 68492, 69173, and 69139 were initially assumed to be mixtures of Pb and Na nitrates (Table 6) with possible oxalate content, and little organic content. The DSC-MS data from these samples (Figures 5-8) are characterized by multiple, overlapping dehydration, decarbonation and denitrification reactions; all exothermic in nature. Coeval gas evolution and exothermic energy events correlate to significant mass losses. These reactions may also be quite vigorous: during an early trial run of 68492 one such reaction resulted in a sudden combustion event at 255.7 °C. According to WCRRF personnel, routine operations following waste remediation included the addition of Swheat© to the parent drums, in order to immobilize small amounts of liquids that were left over. Thus, the possibility of contamination of the residual salts with organic components cannot be completely ruled out.

The thermal analysis results presented here are similar to those referenced in Clark and Funk (2015), Britt (2015) and Wilson et al. (2015). In addition, exothermic reactions were accompanied by the release of H_2O, CO_2, NO and NO_2 during the DSC-MS analysis of five of the seven salt residue samples taken from LANL parent drums. Heated to 500 °C, four of the residual salt samples—69120-3, 68492, 69173, and 69139—undergo exothermic reactions that peak between 253 °C and 258 °C (Table 8). Onset temperatures of these reactions vary from 161.7 °C to 223.6 °C, and the dominant species released is H_2O, accompanied by CO_2 and NO. Mass losses during this reaction vary from 13.33 wt. % to 27.42 wt.

%. The dehydration of 68645 (Figure 6) onsets at 160.4-174.4 °C and peaks at 216.3 °C, losing less than 10% of its total mass in the process (Table 7). Three of the residual salt samples (69120-3, 68645 and 69139) undergo a subsequent exothermic reaction that peaks between 305 and 320 °C and releases primarily CO_2, with some coeval NO and H_2O. Mass losses during this reaction vary from 10.38 to 13.43 wt. %. Sample 68492 shows no evidence of a reaction in this temperature region, while 69173 has a small CO_2 gas peak at 304.4 °C which corresponds to an endothermic peak at 302.4 °C. The latter may be indicative of cerussite decarbonation, which is an endothermic reaction known to occur at ~310 °C at low CO_2 pressures (Ball and Casson, 1975; Yamaguchi et al., 1980). Finally, three of the four samples (68492, 68645, 69139) undergo a high temperature reaction between 342 and 366 °C dominated by the release of CO_2, with lesser amounts of NO and little to no H_2O. 68492 and 68645 undergo significant mass loss during this reaction (Table 8), while 69139 loses ~8 wt. %. Minor losses of NO and CO_2, with little or no attendant mass loss, persist above 399 °C in both 69139 and 69173.

The response of residual salts to thermal energy is analogous to combustion reactions involving an organic component and a nitrate-based oxidizer in air (e.g., Wu and Zavarin, 1986; Biteau, 2009). Possible exothermic reactions could include the dehydration and oxidation of the organic constituent (starch), as well as the combustion of the organics via interaction with nitrate. The complete oxidation and breakdown of the organic component is sustained by ambient atmospheric O_2, as well as by O_2 derived from the breakdown of the nitrates (Biteau, 2009):

$$C_6H_{10}O_5 \cdot H_2O + KNO_3 \rightarrow 6\,CO_2 + 6\,H_2O + K_2O + N_2$$

$$C_6H_{10}O_5 \cdot H_2O + 6\,(O_2 + 3.76\,N_2) \rightarrow 6\,CO_2 + 6\,H_2O + 22.56\,N_2$$

The quadrupole MS cannot resolve CO^+ from N_2^+, thus it is impossible to tell if CO^+ is being produced by the incomplete oxidation via reactions analogous to:

$$C_6H_{10}O_5 \cdot H_2O + 12/5(KNO_3) \rightarrow 6\,CO + 6\,H_2O + 6/5(K_2O) + 6/5(N_2)$$

The above exothermic reactions, from Biteau (2009), involve only $K(NO_3)$. However, a different set of reactions, with different onset temperatures, products, and energy releases may occur when mixed nitrate salts of Na, Al, Pb, Fe, etc. are involved.

It is difficult to infer the amount of energy released during the reactions observed in the DSC-MS, though approximations using background values assumed *ad hoc* that bracket the exotherms suggest that the total amount of thermal energy generated is between 1000 and 1500 J/g. Previous studies indicate that thermally-activated exothermic reactions between nitrate salts and various organic materials including cellulose (Wu and Zavarin, 1986; Pourmortazavi et al., 2009), lactose / starch mixtures (Biteau, 2009), and cloth (Hartman et al., 2007; Scheele et al., 2005) typically onset between 150 and 200 °C and peak in the 200 – 350 °C range. The onset and peak temperatures appear to vary as a function of experimental heating rate (Pourmortazavi et al., 2009), oxidizer (nitrate)-to-fuel (organic) mass ratio (Scheele et al., 2007), and the age of the reacting material (Scheele et al., 2005).

Wu and Zavarin (1986) also found a positive correlation between the pH of the nitrate solution used to treat lignocellulose and the onset temperature of the oxidation exotherm. Wu and Zavarin (1986) and Hartman et al. (2007) also observed that reactions with nitrates of III and IV ions such as Fe^{3+} and Ce^{4+} led to markedly lower onset temperatures. Relatively few of these studies also analyzed the gases produced by these reactions, though Scheele et al. (2007) observed that non-explosive gases such as

CO_2 and H_2O were most abundant. Using FTIR spectroscopy, Biteau (2009) identified CO, aldehydes (CH_2O and $C_2H_4O_2$), formic acid (CH_2O_2), and low levels of N_2O and NO_2, in addition to H_2O and CO_2. Some of these gases persisted to higher temperatures, and N_2O appeared only above 400 °C. Re-analysis of the salt residues and the monolith samples for additional gas constituents (C_2H_3, C_2H_5, C_3H_5: *M/z* = 27, 29, and 41) revealed only trace releases at these *M/z* ratios coeval with the major gas release events.

Table 7: Summary of DSC-MS data from 100 °C to 500 °C. Endothermic reactions denoted by blue text.

Sample	Mass Change (wt. %)	DSC (onset/peak °C: heat transfer)	Gas Peaks (°C; species; mass change)
Top Layer Salts			
S802701	-0.3	Peak @ 274.6: endothermic	No corresponding peak
		Peak @315.5: endothermic	No corresponding peak
S813389	-36.06	n.a. / **111.1**: endothermic	No corresponding peak
		No peak	195.5; H_2O (-7.15 wt. %)
		n.a. / >395: endothermic	>500; NO, NO2 (-25.19 wt.%)
Residual Salts			
68492	-41.45	217.0-226.9 / **254.6**: exothermic	~250: H_2O>NO=CO_2 (-27.42 wt.%)
		n.a. / **342.6**: exothermic	347.0: CO_2>NO (-16.03 wt.%)
68645	-46.51	160.4-174.4 / **216.3**: exothermic	210.3: H_2O>NO=CO_2 (-9.31 wt.%)
		240.2 / **305.0**: exothermic	302.5: NO=CO_2=H_2O (-13.43 wt.%)
		348.0 / **365.5**: exothermic	~354: CO_2>>NO (-23.77 wt.%)
69173	-44.46	204.8 **/ 257.7**: exothermic	255.1: H_2O>>CO_2=NO (-19.78 wt.%)
		2 small endo. peaks @ 302.4, 399.2	Small CO_2 peaks @ 304.4, 396.2
69139	-34.56	223.6-234.1 / **253.2**: exothermic	248.1: H_2O>NO=CO_2 (-13.33 wt.%)
		296.3 / **309.8**: exothermic	308.3: CO_2>NO>H_2O (-10.38 wt.%)
		n.a. / **348.1**: exothermic	361.4: NO=CO_2 (-7.99 wt. %)
		No peak	473.9: NO only (-2.86 wt.%)
Monolith Samples from drum S855793			
69120-1	-26.11	184.0 / **194.2**: exothermic	No gas, no mass change
		203.2 / **238.3**: exothermic	232.3: H_2O (-2.43 wt.%)
		285.6 / **293.1**-**303.6**: exothermic	297.6: CO_2>NO, no H_2O (-14.04 wt.%)
		Shoulder in previous peak	325-330: CO_2>NO, no H_2O (-3.64 wt.%)
		355.0 / **365.9**: endothermic	363.4: CO_2 only (-2.17 wt.%)
		~451.0 / **>500**: endothermic	>500: NO only (-3.83 wt.%)
69120-2	-19.76	157.3 / **184.3**: endothermic	184.8: H_2O only (-1.42 wt.%)
		No peak	233.1: CO_2 only (-2.90 wt.%)
		234.6 / **261.6**: exothermic	No gas
		n.a. / **307.2**: endothermic	305.7: CO_2>NO, no H_2O (-6.09 wt.%)
		n.a. / **328.1**: exothermic	No gas
		340.5 / **347.5**: endothermic	347.5: CO_2 only (-2.72 wt.%)
		n.a. / **378.8**: exothermic	No gas
		n.a. / **435.9**: endothermic	432.5: NO only (-2.38 wt.%)
		467.8 / **497.6**: endothermic	495.6: NO only (-4.19 wt.%)
69120-3	-40.35	161.7-166.6 / **251.4**: exothermic	248.4: H_2O>NO=CO_2 (-19.66 wt.%)
		296.3 / **319.0**: exothermic	314.0: CO_2>NO (-10.57 wt.%)
		Shoulder in previous peak	348.0: NO=CO_2 (-8.06 wt.%)
		Slight rise <500: exothermic	461.9: CO_2 only (-2.06 wt.%)

Finally, onset temperatures may also vary with salt composition, as different combinations of nitrate salts will have eutectic compositions that liquefy well below the melting point of the pure end-members. Chemical analyses (Chamberlin and Martinez, 2015) indicate that the residual salts are primarily mixtures of Pb and Na nitrates, with smaller amounts of Mg, Al, and Ca nitrates (Table 8).

Table 8: Nitrate composition and exothermic onset temperatures for the four residual salt samples.

sample	Pb (Wt. %)	Na (Wt. %)	Mg (Wt. %)	Al (Wt. %)	Ca (Wt. %)	Onset (C°)
68492	21.7	2.73	0.18	0.33	0.26	217.0 - 226.9
68645	18.9	1.61	3.28	2.12	0.27	160.4 - 174.4
69173	42.0	1.39	0.74	0.74	0.16	204.8
69139	24.2	3.72	0.21	0.60	0.25	223.6 - 234.1

The sample with the lowest onset temperature, 68645, also has the most diverse nitrate salt compositions, with >1.0 wt. % each of Na, Mg, and Al nitrates and nitrate hydrates, and a lower Pb nitrate content. The melting points of Pb, Na, Mg, Al, and Ca nitrates (or nitrate hydrates) are, in °C: 270 (Pb), 308 (Na), 88.9 (Mg nitrate hexahydrate) or 129 (Mg nitrate dihydrate), 73.9 (Al nitrate nonahydrate), and 42.7 °C (Ca nitrate tetrahydrate), respectively. Though data on the eutectic compositions for the various binary, tertiary, and higher-order mixtures of these nitrate salts is lacking in the scientific literature, it seems likely that higher contents of the hydrated forms of the divalent and trivalent nitrate salts would tend to lead to lower eutectic temperatures. Nitrate salts, liquefied at lower temperatures, may then react more readily with the organic components in the residual salts. This could also lead to lower onset temperatures for the exothermic oxidation of the organics by nitrates.

In summary, the thermal behavior of the four residual salt samples (68645, 68492, 69173, 69139) is broadly similar, characterized by exothermic dehydration / decarbonation / denitrification reactions having onset temperatures between 160 and 235 °C. Subsequent higher temperature exothermic reactions have onset temperatures between 240 and 350 °C, and release primarily CO_2 and NO_x.

Residual Salt Monoliths from Parent Drum S855793

A third set of samples (69120-1, 69120-2, and 69120-3, see also Figure 10) has a much more diverse mineralogy than the other salt residue samples (Martinez et al, 2015). The DSC-MS data from these samples are also very complex. Sample 69120-1, though primarily composed of a mixture of Na and Pb nitrates, also contains lead nitrate oxalate, $Pb_2(NO_3)_2(C_2O_4)$ and lead oxide, PbO_2. Results from previous studies on the thermal behavior of the constituent compounds identified by XRF are summarized in Table 8. Results of the DSC-MS analysis reveal a complex succession of moderate endothermic and exothermic reactions an order of magnitude less vigorous than those observed during the analysis of the residual salts. Gas release is strongly dominated by CO_2 emission, with lesser amounts of NO and almost no H_2O above ~300 °C.

Thermal analysis of lead nitrate oxalate hydrate, (Boudaren et al., 2001) shows that—after dehydration below 150 °C—the nitrate oxalate breaks down into three phases: lead nitrate $Pb(NO_3)_2$, anhydrous lead oxalate PbC_2O_4, and amorphous, anhydrous $Pb_2(NO_3)_2(C_2O_4)$. Boudaren et al. (2001) postulate that the crystallization of anhydrous $Pb_2(NO_3)_2(C_2O_4)$ occurs between 162 °C and 180 °C, as evidenced by a small exothermic peak with no attendant mass change in this region. In sample 69120-1, a similar transformation could be responsible for a small exothermic peak which onsets at 182.0 °C and peaks at 194.2 °C. $Pb_2(NO_3)_2(C_2O_4)$ then breaks down below 200 °C into $Pb(NO_3)_2$ and PbC_2O_4, both of which, in turn, break down rapidly between ~260 °C and 280 °C, resulting in a significant mass loss. Significant

mass losses occur in both monolith samples 69120-1 and 69102-2 over the same temperature range. Boudaren et al. (2001) further speculate that an exothermic peak at 315–320 °C accompanying the breakdown of lead oxalate into Pb_2OCO_3 may instead result from the oxidation of CO emitted by the sample. Both Pb nitrate and oxalate break down into ever more complex mixed oxynitrates and oxycarbonates which then break down into various Pb oxides (Boudaren et al., 2001). The intermediate compound, $Pb_6O_5(NO_3)_2$, for example, persists to ~335 °C, yielding a mixture Pb_2O_3 and PbO.

Table 9: Thermal properties of the mineral constituents of salt residues from parent drum S855793 (samples 69120-1, 69120-2, and 69120-3).

Constituent	T_{melt} (C°)	T_{boil} (C°)	Characteristics
$NaNO_3$	308	380	Melts, then decomposes to $NaNO_2$, releasing O_2
$NaNO_2$	271	--	Decomposes in air above 320 °C: $2NaNO_2 \rightarrow Na_2O + NO + NO_2$
Na_3ONO_2	--	--	No data – extremely hygroscopic, breaks down to $NaNO_3$, NaOH, and/or $Na_2(CO_3)$ upon exposure to air
$MgCO_3$	--	--	*Anhydrous*: decomposes above 350 °C: $MgCO_3 \rightarrow MgO + CO_2$ *Hydrous*: dehydrates between 157 °C and 179 °C depending on degree of hydration
$Pb(NO_3)_2$	270	--	Decomposes in air above ~300 °C: $2Pb(NO_3)_2 \rightarrow 2PbO + 4\ NO_2 + O_2$
$PbCO_3$	--	--	Decomposes in air above ~200 °C: $2Pb(CO_3) \rightarrow Pb_2OCO_3 + CO_2$ Further decomposition above~310 °C: $Pb_2OCO_3 \rightarrow 2PbO + CO_2$
$Pb_2(NO_3)_2(C_2O_4)\cdot 2H_2O$			Dehydrates 100-150 °C; then breaks down into $Pb(NO_3)_2 + PbC_2O_4$ + complex Pb nitrate & carbonate oxysalts. PbC_2O_4 decomposes between 310-315 °C
PbO_2	--	--	Decomposes above 290 °C: $PbO_2 \rightarrow Pb_{12}O_{19} \rightarrow Pb_{12}O_{17} \rightarrow Pb_3O_4 \rightarrow PbO$ First at 290 °C, second at 350 °C, third at 375 °C and fourth at 600 °C
Pb_2OCO_3			A thermal decomposition product of cerussite (e.g., Ware and Bayliss, 1962; Grisafe and White, 1964; Pring, et al., 1990), Pb_2OCO_3 decomposes above~310 °C: $Pb_2OCO_3 \rightarrow 2PbO + CO_2$

Sample 69120-1 displays a variety of thermochemical trends similar to those noted above. There is significant mass loss between 262.6 °C and 316.3 °C, accompanied by the emission of copious amounts of CO_2 and NO (but no H_2O). Two exothermic peaks occur within this temperature range, at 293.1 °C and 303.6 °C. The latter has a 'shoulder' on its high-temperature leg indicative of an additional reaction (Figure 10) which likely corresponds to the release of NO and CO_2 between 324 – 330 °C. These phenomena may mirror the combined effects of the decarbonation of lead oxalate and the breakdown of $Pb_6O_5(NO_3)_2$ observed by Boudaren et al. (2001). However, the signal at m/z=16 (Figure 11) rises in parallel with CO_2 between 262.6 °C and 316.3 °C. If the signal at m/z=16 is indicative of oxygen, even as a fragment ion of CO_2 or NO_x (in the near total absence of H_2O), it would follow that no oxygen-consuming reactions—such as the oxidation of CO—are taking place in this temperature interval. However, it is also possible that the amount of CO generated by the reaction is miniscule, or that the signal at m/z=16 could also indicate the evolution of isobars such as CH_4^+ or NH_2^+. Unfortunately, we can only speculate on the significance of $Pb_2(NO_3)_2(C_2O_4)$ breakdown *vis a vis* the thermochemistry of sample 69120-1 as quadrupole mass spectrometry offers no way to evaluate CO emission, which is completely obscured by ambient N_2. A final CO_2 peak at 363.4 °C corresponds to a mass loss of 2.17% (Figure 10), and may be

related to the breakdown of PbC_2O_4 (Gavris et al., 2010) produced, in turn, by the breakdown of the mixed oxalate-nitrate. The sample begins to denitrify above 451 °C, much like the top layer salt sample S813389.

The DSC-MS results from sample 69120-2 (Figure 11) are similar in many respects to those of 69120-1, despite its more diverse mineralogy. XRD data revealed the presence of cerussite ($PbCO_3$), and sodium nitrite (+ amorphous material) as primary constituents, with minor amounts of $NaNO_3$, $Pb(NO_3)_2$, shannonite ($Pb_2O(CO_3)$), sodium nitrate oxide ($Na_3O(NO_2)$), and magnesite ($Mg(CO_3)$). Unlike 69120-1, the endothermic dehydration of 69120-2 at ~184 °C yields a copious amount of H_2O, though little to no water is released at higher temperatures. The CO_2 peaks at ~305.7 °C and 347.5 °C correspond to endothermic peaks and may represent the decarbonation of cerussite and magnesite, respectively, and possibly the breakdown of PbC_2O_4 (e.g., Gavris et al., 2010) though the latter may appear exothermic due to the oxidation of the emitted CO. The melting of $NaNO_3$ and/or the breakdown of sodium nitrite and lead nitrate may be responsible for the broad NO peak at ~310 °C. Experiments by Bauer et al. (2009) show that molten Na nitrate reacts with graphite, resulting in the emission of both NO and CO_2 above 300 °C. A similar phenomenon may facilitate the release of NO in this sample at ~310 °C, though the large NO peaks at 432.5 °C and 495.6 °C corresponding to endothermic reactions at 435.9 °C and 497.6 °C show no coeval CO_2 emissions. Thus it seems possible that the high-temperature NO peaks are related to the final breakdown of Pb and Na nitrates into their corresponding oxides.

Studies of $Pb(NO_3)_2$ by Vratny and Gugliotta (1963), and Cram and Davies (1976) indicate that its thermal decomposition proceeds in a stepwise manner over a very broad temperature range (<100 °C – 555 °C), with each reaction releasing NO, NO_2 and O_2 in varying proportions until all that remains is Pb_2O_3 and/or PbO_2. In particular, the 'Stage 5' and 'Stage 6' breakdown of Pb oxynitrates postulated by Cram and Davies (1976) fall close to the peak temperatures observed for high temperature NO emission from 69120-2. Conversely, both Jackson et al. (1995) and L'vov and Novichikhin (1995)—working with a small volume of $Pb(NO_3)_2$ solution deposited on graphite—observed a large NO peak at ~375 °C during $Pb(NO_3)_2$ breakdown, which was not seen in this study. Performing a similar experiment, with similar starting materials, Jackson et al. (1995) also observed smaller NO peaks at ~440 °C and ~480 °C. Hoshino et al (1981) and Radhakrishnan Nair (1988) show that the activation energy and onset temperatures of the thermal breakdown in both $NaNO_3$ and $Pb(NO_3)_2$ decrease in the presence of metal oxide catalysts such as TiO_2, Al_2O_3, Cu_2O, and MnO_2.

Unlike 69120-1 and 69120-2, monolith sample 69120-3 (Figure 12) displayed completely different properties in response to thermal analysis, in terms of reactivity, mass loss, and gas release. In short, despite its mineralogical similarities to 69120-1 (Na and Pb nitrates, plus small amounts of PbO_2 and $Pb_2(NO_3)_2(C_2O_4)$) its response was very similar to that observed in samples 68645, 68492, 69173, and 69139 (Table 7). This may simply indicate that 69120-3 contains a larger organic load than either 69120-1 or 69120-2, and its thermal profile is thus dominated by exothermic outgassing and combustion of an organic constituent in the presence of nitrates. The markedly lower onset temperature of the first exothermic combustion reaction, (161.7 – 166.6 °C) is similar to that observed in 68645. Unlike 69120-1 and 69120-2, which showed little CO_2 emission above ~375 °C and continued to outgas NO_x to 500 °C, 69120-3 showed significant CO_2 emission at high temperature, suggesting a greater organic content, overall. The lack of significant NO and NO_x outgassing above ~400 °C was also characteristic of three of the four residual salt samples: 69173, 68645, and 68492.

The Significance of Sodium Nitrite and Shannonite

It should be noted that several of the compounds identified by XRF (Martinez et al., 2015) in the monolith samples may be produced during various stages of the thermal decomposition of $NaNO_3$ and $PbCO_3$. Sodium nitrite ($NaNO_2$), lead dioxide (PbO_2), and the lead oxycarbonate shannonite (Pb_2OCO_3) were identified in the monolith samples. Sodium nitrite, also a possible primary constituent within the top layer salts, is a common product of the thermal decomposition of sodium nitrate (e.g., Kramer, et al. 1982), though the temperature of the nitrate-to-nitrite reaction is dependent on multiple factors.

In nature, lead dioxide and lead oxycarbonate are rare, but may form during the thermal decomposition of cerussite (e.g., Warne and Bayliss, 1962; Grisafe and White, 1964). Pring, et al. (1990) identified the mineral form of Pb_2OCO_3, shannonite, in loose fill material from a lead mine in New South Wales, Australia where it formed pseudomorphs after well-formed cerussite crystals. This fill material was heated to <390 °C during a well-documented underground mine fire early in 1906. If the cerussite in the waste drum formed as a result of the interaction between oxalic acid and the Pb metal drum shielding, the possibility of a precursor thermal event before the drum was emptied to create drum 68660, may warrant further inquiry.

CONCLUSIONS

In FY2015, MET-1 and NCO-4 were contracted to perform Differential Scanning Calorimetry coupled with quadrupole Mass Spectrometry (DSC-MS) analyses as part of the analytical chemistry effort in support of the investigation of the WIPP Waste Drum failure that occurred on Valentine's Day, 2014. Initially, we examined the thermal behavior of pure, reagent-grade nitrate salts (Na, Pb, K) and nitrate salt hydrates (Fe and Mg) in order to identify the possible waste constituents, which would be most likely to release NO_x at low temperatures. We followed this study up with systematic analyses of four samples sent to us by C-AAC: 2 top layer salts, four residual salts sampled from otherwise empty parent waste barrels that were related in terms of content and time to the salt wastes placed into the drum (68660) that heated and pressurized, and further set of 3 salt residue monolith samples from a single parent drum, S855793, which was a precursor to drum 68660.

The results of these analyses ultimately pose more questions than they answer. However, from the limited set of data available at this time, we can derive several pertinent conclusions:

1) Of the pure nitrate samples analyzed, only Fe^{3+} nitrate hydrate releases NO_x below 200 °C when heated.
2) The thermal behavior of $NaNO_3$, when mixed with low levels (^{235}U = 1600 μg/g; ^{238}U = 840 μg/g; and 1 μg/g or less of ^{239}Pu, ^{237}Np, and ^{241}Am) of radioactive constituents, appears to be identical to that of the pure, unadulterated salt.
3) The thermal response of mixed nitrate salts (e.g., Na + Mg nitrate) is very different from that of the pure end-members.
4) Chemical transformations in nitrate salts and calcium oxalate are endothermic. However, the reactions observed in 5 of the 7 salt residue samples were strongly exothermic, with onset temperatures >160 °C.
5) Exothermic reactions observed in the salt residues release H_2O, CO_2 and NO_x, and strongly resemble those commonly observed in combustion reactions involving mixtures of nitrates and organics.

6) The mineralogy and, to a lesser extent, the thermal behavior of two samples, 69120-1 and 69120-2, suggests that they may have experienced heating and decarbonation prior to the initiation of thermal analysis.

Samples for thermal analysis by DSC-MS were first dried to 110 °C and ground into fine powders to reduce sampling bias. Thus, this effort was inherently not as effective as hoped in terms of identifying which waste phase could have self-heated or ignited at ambient temperatures. However, the conclusions listed above lay the groundwork for follow-on studies.

ACKNOWLEDGEMENT

Thanks to Daniel Garcia, Judy Roybal, Leonard Lujan, and Chastity Kolar (NCO-4) for their assistance during the course of the analytical work that comprises the bulk of this report. A debt of gratitude is also owed to Drs. Joshua White (MST-7), Kirk Veirs (MET-1), Kirk Weisbrod (AET-5), Rebecca Chamberlin (C-AAC), Patrick Martinez (C-AAC), Philip Leonard (M-7), and Paul Schumann (EM) for thorough and insightful technical reviews. The input of each of these individuals significantly improved the content of this report.

REFERENCES

MC **Ball**, MJ Casson (1975) J. Inorg. Nucl. Chem., 37, 2253-2255.
T **Bauer**, D Laing, U Kröner, R Tamme (2009) "Sodium Nitrate for Latent High Temperature Heat Storage" *in*: The 11th International Conference on Thermal Energy Storage – Effstock 14-17 June 2009 in Stockholm, Sweden.
H **Biteau** (2009) "Thermal and Chemical Behaviour of an Energetic Material and a Heat Release Rate Issue" Ph.D Dissertation, University of Edinburgh, 392 p.
C **Boudaren**, J-P Auffrédic, P Bénard-Rocherullé, D Louër (2001) Solid State Sciences, 3, 847–858.
AJ **Bracuti** (1992) "The Crystal and Molecular Structure of Triethanolammonium Nitrate" U.S. Army Armament Research, Development and Engineering Center, Armament Engineering Directorate, Technical Report ARAED-TR-92026, 25p.
K-H **Breuer**, W Eysel (1982) Thermochim. Acta, 57, 317-329.
PF **Britt** (2015) "Oak Ridge National Laboratory Analysis of Waste Isolation Pilot Plant Samples: Integrated Summary Report" ORNL/LTR-2015/203, March 2015, 30 p.
RM **Chamberlin**, PT Martinez (2014) "Drum Sampling and Analysis" LA-UR-14-26884.
RM **Chamberlin**, PT Martinez and others (2015) "Analytical Chemistry and Materials Characterization Results for Debris Recovered from Four Nitrate Salt Waste Drums" LA-UR-15-26850.
DL **Clark** (2015) "Characterization of the Potential Hazards Associated with Potential RCRA Treatment Noncompliances" LA-UR-15-26595.
DL **Clark**, DJ Funk (2015) "Chemical Reactivity and Recommended Remediation Strategy for Los Alamos Remediated Nitrate Salt (RNS) Wastes" LA-UR-15-22393.
AG **Cram**, MB Davies (1976) J Inorg. Nucl. Chem. 38, 1111-1117.
LR **Drake** (2014) "Analytical Results from the Area G Nitrate Salt Samples Submitted to C-AAC" LA-UR-14-26900.
MAA **El Masry**, A Gaber, EMH Khater (1998) J. Therm. Anal. 52, 489-495.
AM **Gadalla** and H-F Yu, 1990 J. Mater. Res., Vol. 5, No. 6, Jun 1990 1233-1236
G **Gavris**, M Stoia, O Stanasel, S Hodisan (2010) Chem. Bull. "POLITEHNICA" Univ. (Timisoara), 55(69), 143-147.

DA **Grisafe**, WB White (1964) Am. Mineral., 49, 1184-1198.
JR **Hartman**, CA Waters, CL Beyler (2007) Fire Mater., 31, 359–371.
Y **Hoshino**, T Utsunomiya, O Abe (1981) Bull. Chem. Soc. Japan, 54, 1385-1391
JG **Jackson**, RW Fonseca, JA Holcombe (1995) Spectrochimica Acta Part B-Atomic Spectroscopy, 1995 Oct, Vol.50(12), pp.1449-1457
CM **Kramer**, ZA Munir, JV Volponi (1982) Thermochim. Acta 55, 11-17.
BV **L'vov**, AV Novichikhin (1995) Spectrochimica Acta Part B 50 (1995) 1427-1448
PT **Martinez**, RM Chamberlin, DS Schwartz, and others (2015) "Analytical Chemistry and Materials Characterization Results for Debris Recovered from Nitrate Salt Waste Drum S855793," LA-UR-15-27132, 23 p.
J **Mu** and DD Perlmutter (1982) Thermochimica Acta 56, 252-260.
SM **Pourmortazavi**, SG Hosseini, M Rahimi-Nasrabadi, SS Hajimirsadeghi, H. Momenian (2009) J. Haz. Mat., 162, 1141–1144.
A **Pring**, WD Birch, A Reller (1990) Mineral. Mag., 54, 647-649.
TD **Radhakrishnan Nair** (1988) React. Kinet. Catal. Lett., Vol. 36, No. 2, 351-355 (1988)
RG **Reddy**, T Wang, D Mantha (2012) Thermochim. Acta , 531, 6– 11.
RD **Scheele**, DS Trent, TD Cooper, MK Edwards, SA Jones, AE Kozelisky, JR Ewalt, PA Scott, JA Compton, MJ Minette (2005) "Thermal Stability Studies of Candidate Decontamination Agents for Hanford's Plutonium Finishing Plant Plutonium-Contaminated Gloveboxes" PNNL-15410, September 2005.
RD **Scheele**, BK McNamara, LM Bagaasen, SJ Bos, AE Kozelisky, PK Berry (2007) "Evaluation of Exothermic Reactions from Bulk-Vitrification Melter Feeds Containing Cellulose" PNNL-16677, April 2007.
PB **Schumann** (2015) Internal LANL e-mail communication.
F **Vratny**, F Gugliotta (1963) J. lnorg, Nucl. Chem., 1963, Vol. 25, pp. 1129 to 1132.
S St.J **Warne**, P Bayliss, 1962 Am. Mineral., 47, 1011-1023.
K **Wieczorek-Ciurowa** and AJ Kozak (1999) J. Therm. Anal. Cal., 58, 647-651
DL **Wilson**, ML Baker, BR Hart, JE Marra, JM Schwantes, PE Shoemaker (2015) "Waste Isolation Pilot Plant Technical Assessment Team Report," March 17, 2015, SRNL-RP-2014-01198, Revision 0, 277 p.
K-T **Wu**, E Zavarin (1986) Thermochim. Acta, 107, 131-148.
J **Yamaguchi**, Y Sawada, O Sakurai, K Uematsu, N Mizutani, N Kato (1980) Thermochim. Acta, 35, 307-313.

ADDENDUM

DSC-MS Analysis of Mixtures of Tri- and Divalent Nitrate Hydrate Salts and Oxalic Acid

Following the compilation and synthesis of the DSC-MS data for pure nitrates, top layer salts, residual salts, and residual salt monoliths from unremediated LANL parent drums, we decided to explore the thermal response of oxalate / nitrate mixtures to determine if the carbon contributed by the oxalate (as crystalline oxalic acid hydrate) would react exothermically with gaseous NO_x emitted during the thermal breakdown of trivalent and divalent nitrate hydrates of Al and Fe(III). This would presumably involve the cleavage of the C-C bond in oxalic acid, a C2 compound, to form CO_2. Little work has been documented on the nature of reactions between oxalates (or oxalic acid) and nitrate salts at high temperature. Kubota (1982) reports the Mn-catalyzed breakdown of oxalate ions in HNO_3 solutions below 100 °C.

Oxalic acid is commonly manufactured by the oxidation of carbohydrates with nitric acid. Pure, anhydrous oxalic acid melts and decomposes at 187 °C, though it begins to sublimate slightly below 100 °C. The dihydrate, if heated rapidly, melts at 101.5 °C. If heated slowly, it dehydrates to the anhydrous form at the same temperature. Upon heating, oxalic acid decomposes to formic acid, carbon monoxide, carbon dioxide, and water (Sawada and Murakami, 2000).

Pure reagent-grade oxalic acid hydrate, and Al and Fe(III) nitrate hydrates were obtained from LANL's M-7 group. Samples were prepared by weighing equimolar masses of each nitrate hydrate and oxalic acid hydrate and grinding each pair to a fine powder using a clean agate mortar and pestle. Additionally, two samples utilizing a 10:1 mixture of Al nitrate hydrate and oxalic acid were analyzed. A small quantity (10 – 40 mg) of each mixture was transferred, using a stainless steel spatula, into a clean platinum-rhodium (Pt-Rh) STA pan, placed on the DSC carrier and covered with a pierced Pt-Rh lid. When mixed with oxalic acid, Fe(III) nitrate hydrate spontaneously sorbed water and turned into a canary-yellow paste. The DSC-MS run described here used the hydrated paste as the starting material. In the dry air glovebox environment, the remaining unanalyzed paste dehydrated and turned into a dull yellow powder in a matter of hours.

During analysis, ambient glovebox conditions were: temperature (T) = 25 to 30 ^{o}C, relative humidity (%RH) = 0.0 – 1.0%. Pre-run baseline values varied from approximately -5.5 to -4 μV. For all nitrate / oxalic acid mixtures, temperature Profile 4 was used (Table 3) and the run was stopped manually at 500 °C. Unless otherwise indicated, all other analytical parameters for the nitrate/oxalate acid samples were identical to those used for the analysis of the samples described in the main body of this report.

$Al(NO_3)_3{\cdot}9H_2O$ / $C_2H_2O_4{\cdot}2H_2O$ – 10:1 molar ratio: The thermal behavior of 10:1 molar mixtures of Al nitrate nonahydrate and oxalic acid dihydrate are (Figure 13), as one would expect, dominated by the thermal behavior of the nitrate itself. In the first sample, run immediately after mixing, endothermic melting (onset = 45.3 °C) and dehydration (onset = 107.3 °C) reactions dominate below ~210 °C; the latter releasing copious amounts of H_2O (peak = 123.8 °C) and minor amounts of NO. These reactions run to completion at ~190 °C, at which point the mixture has lost 55.72% of its initial mass. Three subsequent reactions, one mildly endothermic and two mildly exothermic release mostly NO and CO_2 in varying amounts. The first onsets at 212.9 °C, releasing both NO (peak = 217.2 °C) and CO_2 (peak = 214.9 °C), and corresponds to a further mass loss of 10.53 wt. %. The two exothermic peaks onset at 282.3 and 326.2 °C and both release CO_2. These reactions result in additional mass losses of 10.62 wt. % and 5.10 wt. %, respectively.

Figure 13: DSC-MS data (to 500 °C) for 10:1 molar mixture of $Al(NO_3)_3 \cdot 9H_2O$ and oxalic acid.

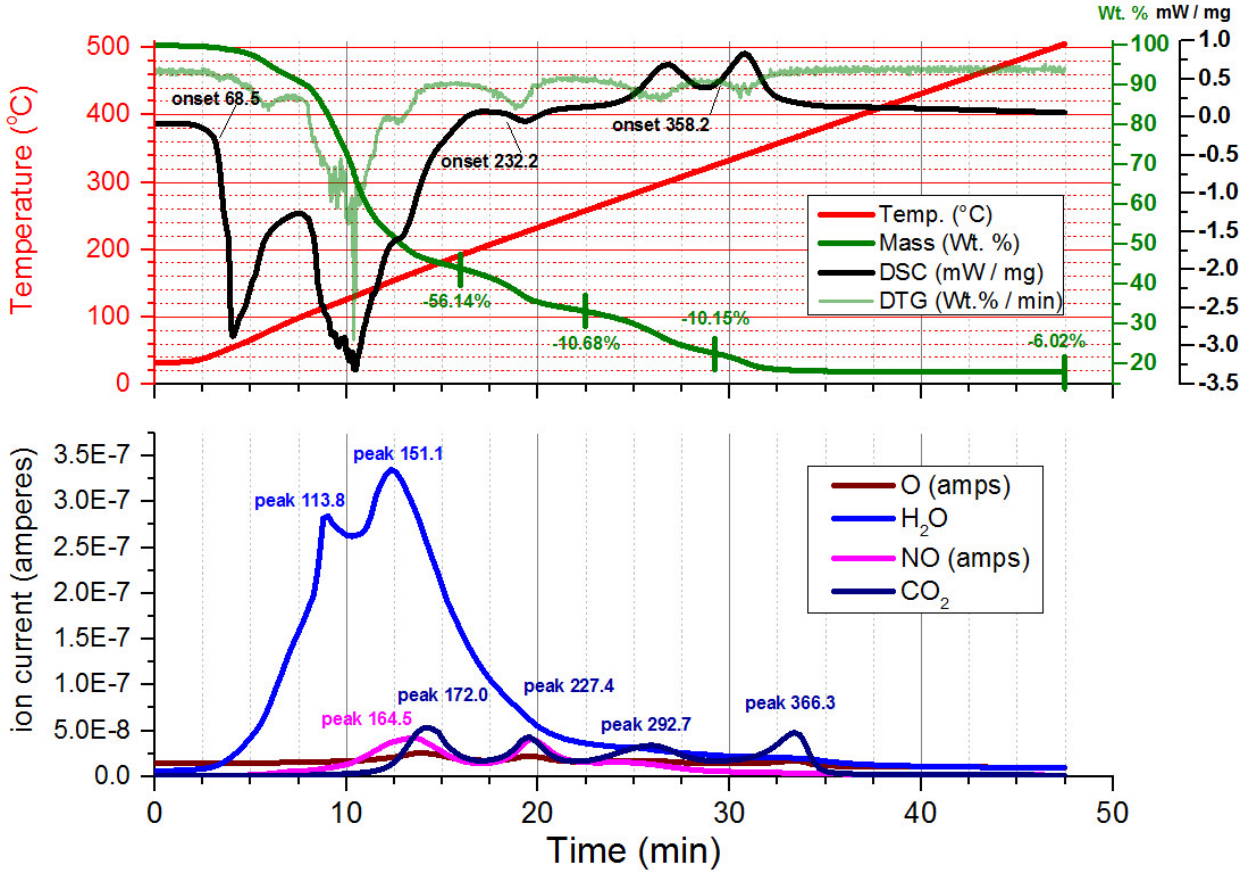

A duplicate sample run several hours later (Figure 13) yields results that are slightly different in several respects. Melting onsets at a higher temperature (68.5 °C), and dehydration occurs in two discrete H_2O pulses which peak at 113.8 °C and 151.1 °C. The small endothermic peak also onsets at a slightly higher temperature (232.2 °C) and is barely visible, as do the two CO_2-emitting exothermic reactions. Gas releases follow a similar sequence, however, with minor NO emission coeval with dehydration, followed by three discrete pulses of CO_2, the first of which is accompanied by significant NO emission. Mass losses in this sample were nearly identical: -56.14 wt. %; -10.68 wt. %; -10.15 wt. %; and 6.02 wt. %.

$Al(NO_3)_3 \cdot 9H_2O$ / $C_2H_2O_4 \cdot 2H_2O$ – 1:1 molar ratio: When the oxalic acid content is increased to achieve an equal molar ratio with the aluminum nitrate nonahydrate, the behavior of the sample at temperatures below ~200 °C is, again, dominated by the thermal response of $Al(NO_3)_3 \cdot 9H_2O$ to increasing temperature (Figure 14). Endothermic melting onsets at 45.8 °C, followed by multiple dehydration events (H_2O peaks at 147.5 °C and 199.4 °C), the first of which releases both NO and CO_2. A subsequent dehydration releases a greater amount of CO_2, indicating that the oxalic acid is also beginning to break down. Though there may be as many as four discrete H_2O peaks, mass loss proceeds in 2 easily-resolvable steps: -46.52 wt.% complete at 161.8 °C and a further -36.37 wt. % complete at 230.1 °C. Above ~230 °C, the enthalpy plateaus close to 0 to ~300 °C, where an exothermic reaction releasing only CO_2 onsets at 330.3 °C. This final CO_2 release corresponds to a mass loss of 8.70 wt. %. A second exothermic peak that follows the first may be indicative of CO oxidation, as the oxygen concentration of the offgas drops precipitously, immediately prior to the development of this peak (Figure A2).

A duplicate sample run several hours later produced somewhat different results, though melting onsets at a higher temperature (63.5 °C), and dehydration occurs in two discrete H_2O emissions which peak at 117.8 °C and 207.7 °C, each accompanied by a discrete endothermic reaction. Mass loss after the first dehydration is 15.63 wt. %, and a further 68.68 wt. % is lost after the second dehydration, which is complete at ~236 °C. Unlike the initial run, significant amounts of CO_2 and NO are also released during the second dehydration reaction. Additional CO_2 and O are evolved during a significant exothermic reaction which onsets at 353.3 °C. The final CO_2 release corresponds to a mass loss of 9.04 wt. %, and lacks the ancillary CO oxidation peak.

Figure 14: DSC-MS data (to 500 °C) for 1:1 molar mixture of $Al(NO_3)_3 \cdot 9H_2O$ and oxalic acid.

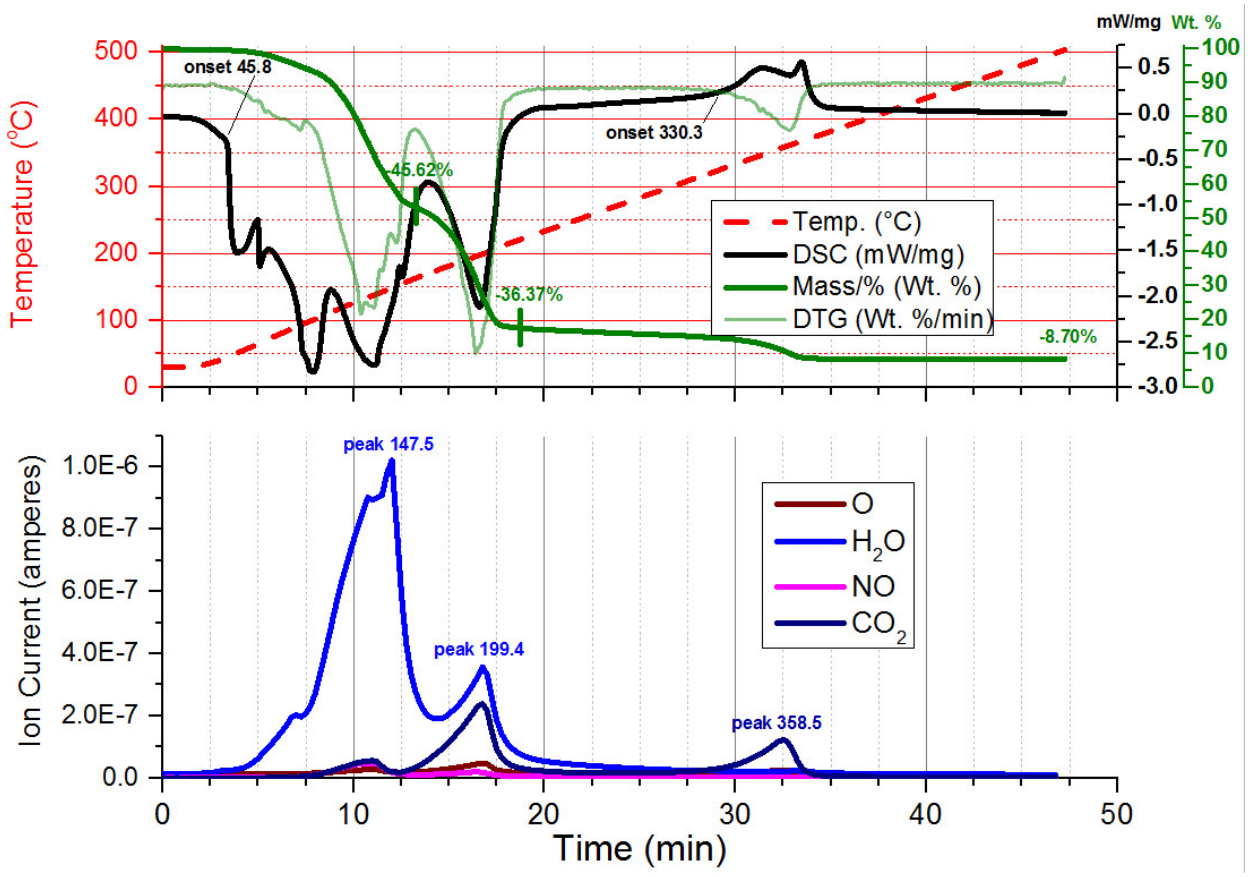

<u>$Fe(NO_3)_3 \cdot 9H_2O$ / $C_2H_2O_4 \cdot 2H_2O$ – 1:1 molar ratio:</u> The equimolar mixture of oxalic acid dihydrate and ferric nitrate nonahydrate produces results which are quite similar to those seen in the equimolar mixture with aluminum nitrate nonahydrate. Below ~230 °C, the most significant features consist of the endothermic melting and multi-step dehydration of the ferric nitrate (Figure 15). These reactions are immediately followed by a broad, plateau-like exothermic reaction which onsets at 231.7 °C and peaks at 268.6 °C. This reaction is complete at ~324.8 °C, and is dominated by CO_2 release. The release of formic acid (CO_2H_2) between ~210 and 230 °C is evident by the decoupling of the NO peak from the peak at m/Z = 46, which corresponds to NO_2 for most of these analyses. Here, the rise of m/Z=46 tracks the evolution of H_2O, H_2, and CO_2 produced by the possible breakdown of ferrous oxalate, rather than that of NO (Figure 16).

Discussion: Oxalic – Nitrate mixtures

The few experiments run using mixed trivalent nitrate salts and oxalic acid indicate that oxalic acid is not oxidized exothermically by NO_x released as the nitrate breaks down. Instead, the oxalic acid breaks down exothermically at higher temperatures, releasing formic acid, CO_2, CO, and H_2O. As with pure nitrate salts, the enthalpy profile of these mixtures below ~210 °C is dominated by endothermic phase changes, dehydration / denitrification reactions and the formation of metal oxalates.

Figure 15: DSC-MS data (to 500 °C) for 1:1 molar mixture of $Fe(NO_3)_3 \cdot 9H_2O$ and oxalic acid.

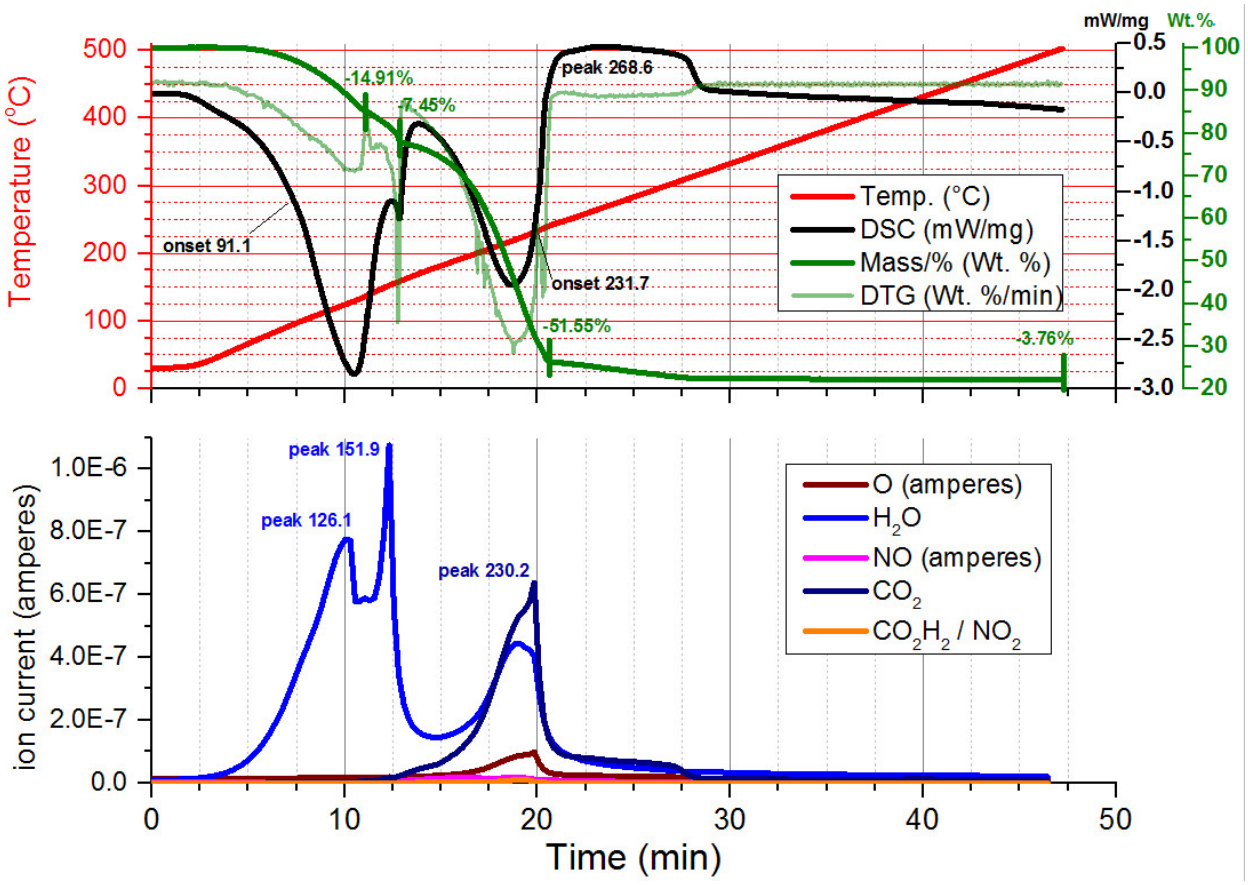

The persistence of oxalate in some form in the Al nitrate/oxalic acid is suggested by the exothermic reactions which onset at ~330-360 °C. Though pure oxalic acid breaks down below 200 °C, Palaniappan (1995) also noted a the occurrence of a broad exotherm above 210 °C in mixtures of oxalic acid and polyaniline salts which was attributed to the breakdown of the oxalic acid. Broadbent, et al (1967) observed exothermic peaks just below 300 °C in ferrous oxalate heated in air. When heated in nitrogen, the same compound yielded a flat-topped plateau in the same temperature range that resembles the one seen in Figure 15, above. Other transition metal oxalates decompose to CO_2, CO, H_2O and the corresponding metal oxide in air between ~240 and 460 °C (Mohamed et al, 2005). For ferrous oxalate hydrate, Mohamed et al. (2005) observed an exothermic peak at 244 °C, which coincided to the compound's breakdown into iron oxides. In the case of the aluminum nitrate / oxalic acid mixtures, the formation of aluminum oxalate during the breakdown of the nitrate and oxalic acid seems likely, as other investigators (e.g., Kumar Saha and Pramanik, 1994) have noted that aluminum oxalate reacts exothermically, breaking down at ~375 °C.

Figure 16: Decoupling of m/Z=46 from m/Z=30, indicative of formic acid evolution during Fe3+ oxalate breakdown at ~220 °C in the $Fe(NO_3)_3 \cdot 9H_2O$ / oxalic acid mixture.

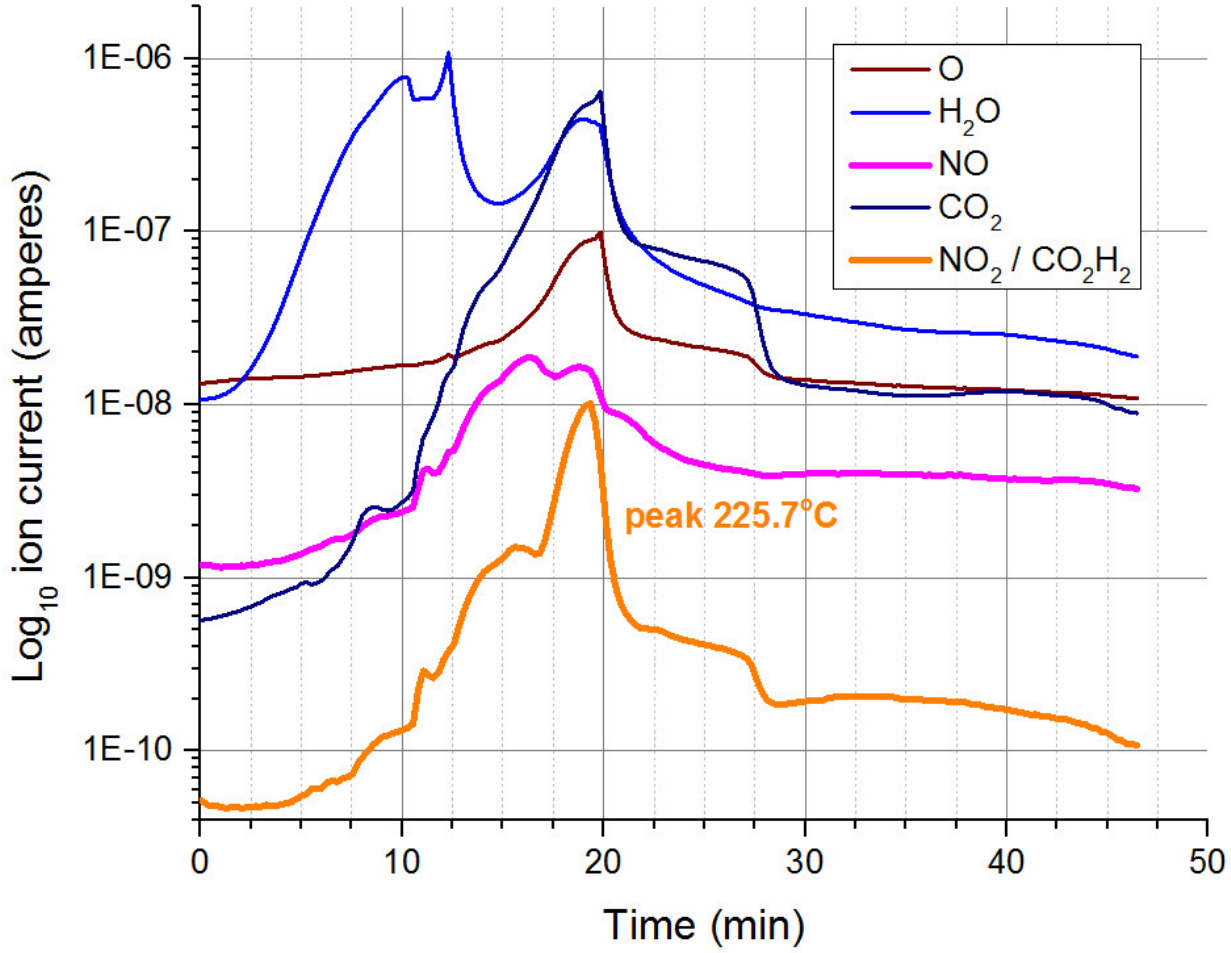

REFERENCES (Addendum)

D **Broadbent**, D Dollimore, J Dollimore (1967) J. Chem. Soc. A, 1967, 451-454.
M **Kubota** (1982) J. Radioanalytical Chem., 75, 39-49.
S **Kumar Saha**, P Pramanik (1994) J. Mater. Sci. 29, 3425-3429.
MA **Mohamed**, AK Galwey, SA Halawy (2005) Thermochimica Acta 429, 57–72.
M **Palaniappan** (1995) J. Polymer Sci. A Polymer Chemistry, 33,2443-2447.
H **Sawada**, T Murakami (2000) "Oxalic Acid" *in*: Kirk-Othmer Encyclopedia of Chemical Technology, John Wiley & Sons, Inc., 19 p.